

RESEARCH ARTICLE

Tectonic significance of the Cretaceous granitoids along the south-east coast of continental China

Qiqi Xue^{1,2}  | Yaoling Niu^{1,2,3,4} | Shuo Chen^{2,3,5} | Pu Sun^{2,3} | Meng Duan^{1,2} |
Yajie Gao^{2,3,5} | Di Hong^{2,3,5} | Yuanyuan Xiao^{2,3} | Xiaohong Wang^{2,3} | Pengyuan Guo^{2,3}

¹School of Earth Science and Mineral Resources, China University of Geosciences, Beijing, China

²Laboratory for Marine Geology, Qingdao National Laboratory for Marine Science and Technology, Qingdao, China

³Institute of Oceanology, Chinese Academy of Sciences, Qingdao, China

⁴Department of Earth Sciences, Durham University, Durham, UK

⁵University of Chinese Academy of Sciences, Beijing, China

Correspondence

Qiqi Xue, School of Earth Science and Mineral Resources, China University of Geosciences, Beijing 100083, China.

Email: xueq0451@foxmail.com

Yaoling Niu, Department of Earth Sciences, Durham University, Durham DH1 3LE, UK.
Email: yaoling.niu@durham.ac.uk

Funding information

National Natural Science Foundation of China, Grant/Award Numbers: 41130314, 41776067 and NSFC41630968; Scientific and Technological Innovation Project Financially Supported by Qingdao National Laboratory for Marine Science and Technology, Grant/Award Number: 2015ASKJ03; 111 Project, Grant/Award Number: B18048; NSFC-Shandong Joint Fund for Marine Science Research Centers, Grant/Award Number: U1606401; Qingdao National Laboratory for Marine Science and Technology, Grant/Award Number: 2015ASKJ03; Chinese Academy of Sciences, Grant/Award Number: Y42217101L

Handling Editor: E. Bozkurt

We present the results of our study on 16 Cretaceous granitoid plutons along the south-east coast of continental China. The zircon U-Pb ages and the bulk-rock Rb-Sr isochron age ($R^2 = 0.935$) indicate that the granitoids represent the last episode of magmatism (119–92 Ma) associated with the paleo-Pacific Plate subduction beneath continental China. These granitoids show large compositional variation that is to a first-order consistent with varying extents of magma evolution, which is best expressed by a large SiO_2/MgO range and correlated trends of SiO_2/MgO with the abundances and ratios of major and trace elements. The correlated Nd ($\epsilon\text{Nd}_{(t)} = -6.1$ to -1.2) and Hf ($\epsilon\text{Hf}_{(t)} = -4.7$ to $+3.4$) isotopic variation reflects parental magma compositional differences as a result of varying sources and processes. The Nd-Hf isotope data indicate that these granitoids were produced by mature continental crust melting with significant mantle input (~20–60%). Rhyolite-MELTS modelling shows that relative to the less evolved (i.e., low SiO_2/MgO) granitoid plutons, the progressively more evolved (i.e., varying larger SiO_2/MgO) plutons can be explained by varying extents (~24% to 67%) of fractional crystallization. The origin of the magmas parental to the granitoids is best explained by a two-stage process: (a) subducting slab dehydration-induced mantle wedge melting for basaltic magmas and (b) ascent and underplating/intrusion of the basaltic magmas caused the mature crustal melting for the granitoid magmas. The systematic northward decrease in $\epsilon\text{Nd}_{(t)}$ and $\epsilon\text{Hf}_{(t)}$ suggests progressively more enriched crustal material towards the north, but it may very well indicate northward crustal thickening, permitting a greater extent of crustal assimilation.

KEYWORDS

Cretaceous granitoids, crustal thickness variation, crust–mantle interaction, paleo-Pacific Plate subduction, south-east continental China

1 | INTRODUCTION

Mesozoic granitoids are widespread throughout south-east continental China (Figure 1; He, Xu, & Niu, 2010; Zhou, Sun, Shen, Shu, & Niu, 2006) and have been studied for almost a century because of their association with mineralization and their implications on geological evolution of the region (Li et al., 2010; Wu, Li, Yang, & Zheng, 2007). At present, their petrogenesis is generally accepted as being associated with

paleo-Pacific Plate subduction (Chen, Yang, Zhang, Sun, & Wilde, 2013; Li & Li, 2007; Li, Qiu, & Yang, 2014; Niu et al., 2015; Yang et al., 2018; Zhao, Qiu, Liu, & Wang, 2016; Zhou & Li, 2000), but many important details remain unaddressed. Following the studies of the Jurassic–Cretaceous granitoid widespread in the interiors of the eastern continental China, Niu et al. (2015) argued that all of these granitoids are of intra-plate origin indirectly associated with the paleo-Pacific Plate subduction, with a scenario of the paleo-Pacific Plate lying horizontally

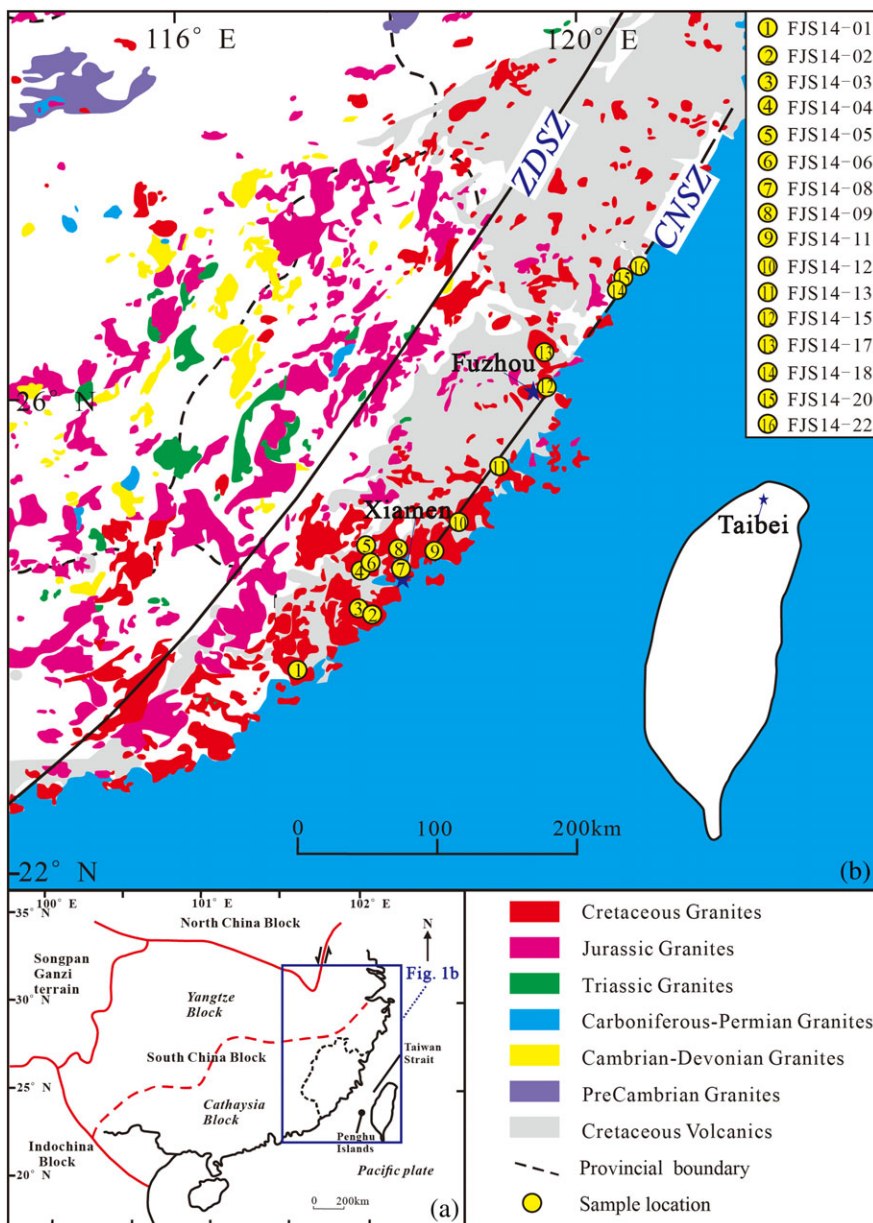


FIGURE 1 (a) Simplified geological map of major tectonic units in south-east continental China (after Chen, Lu, Lin, & Lee, 2006); (b) simplified geological map of south-east continental China, showing the distribution of granitoids and our sample localities along the coast region (after Niu, Shen, Shu, Sun, & Zhou, 2006; Sun, 2006). ZDSZ means Zhenghe-Dapu shear zone; CNSZ means Changle-Nan'ao shear zone [Colour figure can be viewed at wileyonlinelibrary.com]

in the mantle transition zone, whose dehydration provided the water that weakened and thinned the mantle lithosphere with the resulting basaltic magmatism responsible for the intra-plate granitoids. However, the granitoids along the south-east coastline are predicted to have directly derived from the overlying crust caused by mantle wedge basaltic magmatism in response to subducting slab dehydration at the time of, or shortly beforehand, the subduction cessation due to the trench jam by an oceanic plateau/microcontinent (the present-day Chinese continental shelf basement) at ca. 100 Ma (Niu et al., 2015).

The significance of this hypothesis is multifold, and its testing will offer new perspectives on the petrogenesis of granitoids in general and, more specifically, the Mesozoic geology of the western Pacific and eastern Eurasia in a global context. A testable aspect of the hypothesis is that the aforementioned “intra-plate” granitoids and the “subducting”-induced coastal granitoids have different sources and magma evolution histories. These differences must be recorded in the petrology and geochemistry of these granitoids. Here, we report

new geochemical data on the granitoids from the south-east coast of continental China with their age dating results, aiming to (a) explain the petrogenesis of these granitoids; (b) discuss their tectonic implications; and (c) build the basis for comparison with those “intra-plate” granitoids in the interiors of eastern continental China.

2 | GEOLOGICAL BACKGROUND AND PETROGRAPHY DESCRIPTION

2.1 | Geological background

The south-east coast of continental China was once located at an active continental margin of the paleo-Pacific Plate subduction in the Mesozoic (Figure 1a; Li & Li, 2007; Niu et al., 2015; Zhou et al., 2006). The Zhenghe-Dapu shear zone (ZDSZ) and Changle-Nan'ao shear zone (CNSZ) are two main NE-striking faults in the south-east

TABLE 1 Petrography of granitoid samples from south-east coast of continental China ($N = 16$)

Sample	Locality	Latitude, longitude	Altitude (m)	Lithology	Petrographic description
FJS14-01	Zhaohan	23°41'38"N, 117°3'16.9"E	26	Biotite granite	Grey white; medium-grained and coarse-grained; quartz (~30 vol.-%), orthoclase (~40 vol.-%), plagioclase (~25 vol.-%), biotite (~5 vol.-%), Fe-Ti oxides, zircon, apatite
FJS14-02	Huxi	24°9'47.7"N, 117°48'23.4"E	3	Biotite monzogranite	Pale red; medium-grained and coarse-grained; quartz (~25 vol.-%), orthoclase (~35 vol.-%), plagioclase (~35 vol.-%), biotite (~5 vol.-%), Fe-Ti oxides, zircon, apatite, titanite
FJS14-03	Changqiao	24°14'39.3"N, 117°41'44.3"E	10	Biotite granite	Grey white; medium-grained and coarse-grained; quartz (~25 vol.-%), perthite (~45 vol.-%), plagioclase (~25 vol.-%), biotite (3~5 vol.-%), Fe-Ti oxides, zircon
FJS14-04	Chengxi	24°25'12"N, 117°38'12.4"E	5	Alkali feldspar granite	Pale red; medium-grained; quartz (~35 vol.-%), microcline (~50 vol.-%), plagioclase (~15 vol.-%), biotite, zircon, apatite
FJS14-05	Gunong	24°44'22.7"N, 117°43'24"E	60	Biotite monzogranite	Grey; coarse-grained; quartz (~30 vol.-%), orthoclase (~35 vol.-%), plagioclase (~25 vol.-%), biotite (5~10 vol.-%), Fe-Ti oxides, titanite, zircon
FJS14-06	Changtai	24°34'57.8"N, 117°45'46.1"E	7	Granodiorite	Grey; medium-grained; quartz (~25 vol.-%), orthoclase (~25 vol.-%), plagioclase (~30 vol.-%), amphibole (~10%), biotite (~10 vol.-%), Fe-Ti oxides, zircon, titanite, apatite; contain plenty of mafic microgranular enclaves (MMEs)
FJS14-08	Xiamen	24°31'0.8"N, 118°2'22.3"E	4	Biotite granite	Pale red; medium-grained; quartz (~30 vol.-%), perthite (~45 vol.-%), plagioclase (~20 vol.-%), biotite (~5 vol.-%), Fe-Ti oxides, zircon
FJS14-09	Huacuo	24°39'32.7"N, 118°2'2.9"E	3	Biotite granite	Grey; massive and medium-grained; quartz (~35 vol.-%), perthite (~45 vol.-%), plagioclase (~15 vol.-%), biotite (3~5 vol.-%), Fe-Ti oxides, zircon
FJS14-11	Weitou	24°41'13.1"N, 118°22'15.8"E	9	Biotite monzogranite	Light grey; medium-grained; quartz (~20 vol.-%), perthite (~40 vol.-%), plagioclase (~30 vol.-%), biotite (5~10 vol.-%), Fe-Ti oxides, zircon
FJS14-12	Quanzhou	24°54'11.3"N, 118°38'7.6"E	3	Monzogranite	Grey; massive and medium-grained; quartz (~35 vol.-%), microcline (~35 vol.-%), plagioclase (~30 vol.-%), biotite (~1 vol.-%), zircon, apatite
FJS14-13	Putian	25°24'31.3"N, 118°56'33.8"E	97	Monzogranite	Pale red; massive and medium-grained; quartz (~25 vol.-%), perthite (~55 vol.-%), plagioclase (~20 vol.-%), biotite, Fe-Ti oxides, zircon
FJS14-15	Kuiqi	26°00'47.8"N, 119°26'5.5"E	46	Alkali feldspar granite	Grey; massive and medium-grained; quartz (~30 vol.-%), orthoclase (~45 vol.-%), plagioclase (~25 vol.-%), biotite (~1 vol.-%), Fe-Ti oxides, zircon
FJS14-17	Dangyang	26°21'33.9"N, 119°27'28.2"E	146	Granodiorite	Grey; massive and medium-grained; quartz (~20 vol.-%), perthite (~25 vol.-%), plagioclase (~30 vol.-%), biotite (~10 vol.-%), amphibole (~10 vol.-%), Fe-Ti oxides, zircon; contain plenty of MMEs
FJS14-18	Sansha	26°55'45.2"N, 120°09'51.7"E	35	Graphic granite	Pale red; medium-grained and fine-grained; graphic texture; quartz (~25 vol.-%), Fe-Ti oxides, zircon
FJS14-20	Dacengshan	27°0'21.8"N, 120°13'54.7"E	190	Biotite monzogranite	Pale red; massive and medium-grained; quartz (~25 vol.-%), orthoclase (~40 vol.-%), plagioclase (~35 vol.-%), biotite (~1 vol.-%), Fe-Ti oxides, zircon
FJS14-22	Nanzhen	27°7'9.8"N, 120°22'19.5"E	16	Biotite monzogranite	Pale red; medium-grained and coarse-grained; graphic texture; quartz (~25 vol.-%), perthite (~40 vol.-%), plagioclase (~30 vol.-%), biotite (~5 vol.-%), Fe-Ti oxides, zircon

coastal region of our study (Figure 1b; Shu, Yu, & Wang, 2000; Wang & Shu, 2012; Wang, Sun, Chen, Ling, & Xiang, 2013). Our study is focused on the granitoids along, and in the vicinity of, the CNSZ (Figure 1b).

2.2 | Petrography

We collected representative samples from 16 granitoid plutons along the south-east coastline of continental China (Figure 1b). These samples included granodiorite, biotite granite, biotite monzogranite, monzogranite, and alkali feldspar granite. The sample and petrographic details are given in Table 1.

The granodiorite consists of quartz, plagioclase, alkali feldspar, amphibole, biotite, and accessory minerals (e.g., Fe-Ti oxides, zircon, titanite, and apatite; Figures 2a–c). Mafic magmatic enclaves (MMEs) are widespread in the granodiorite and have the same mineralogy as the host. However, the MMEs have greater modal amphibole and biotite than the host (Figure 2a). The biotite granite has varying grain size with a mineral assemblage of quartz, alkali feldspar, plagioclase, biotite, and accessory minerals (e.g., Fe-Ti oxides, zircon, and apatite; Figure 2d). The biotite monzogranite has a mineral assemblage of quartz, alkali feldspar, plagioclase, biotite, and accessory minerals (e.g., Fe-Ti oxides, zircon, apatite, and titanite; Figure 2e). They are exposed as a single pluton or composite granitoid complexes. Most of the alkali feldspar granites are equigranular with a graphic texture and mineral assemblage of quartz, alkali feldspar, plagioclase, biotite, and accessory minerals (e.g., Fe-Ti oxides, zircon, and apatite). Minor arfvedsonite exists in the Kuiqi (FJS14-15) alkali feldspar granite (Figure 2f).

3 | ANALYTICAL METHODS

3.1 | Zircon U-Pb dating

Zircons were extracted using heavy liquid and magnetic techniques, followed by selection under a binocular microscope. The selected zircons were mounted with epoxy and polished to expose the smooth interiors for cathodoluminescence (CL) imaging and photographing under reflected light. The zircon U-Pb dating was done using the LA-ICP-MS method at the Laboratory of Ocean Lithosphere and Mantle Dynamics (OLMD), Institute of Oceanology, Chinese Academy of Sciences. The instrument consists of an Agilent 7900 inductively coupled plasma mass spectrometry (ICP-MS) coupled with a Photon Machine Excite laser ablation system. We chose to perform the laser ablation spot analysis on zircons with oscillatory zoning away from inclusions and cracks. We used the single point ablation method with the working parameters of 193-nm wavelength, 8-Hz repetition rate, energy of 4.24 J/cm², and 35-μm spot size. The data acquisition time for each analysis was 100 s (50 s on background and 50 s on ablated signal). NIST610 was used as the external standard with ²⁹Si as the internal standard. The zircon standard 91500 (Wiedenbeck et al., 1995) was used for quality control (QC) to correct for instrumental drift. The offline data processing was done using ICPDataCal10.4 (Liu et al., 2010). Isoplot 3.0 (Ludwig, 2003) was used for plotting concordia diagrams and calculating the weighted mean ages.

3.2 | Major and trace elements

The whole-rock major element analysis was done using a Leeman Prodigy inductively coupled plasma optical emission spectroscopy (ICP-OES) system at China University of Geosciences in Beijing (CUGB) with

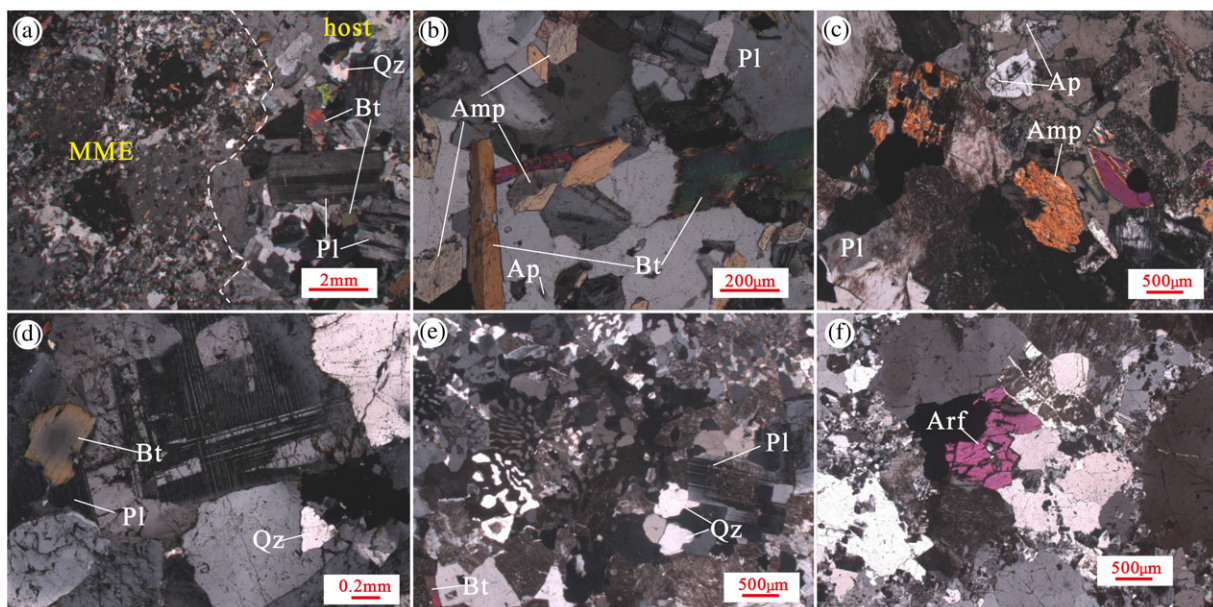


FIGURE 2 Photomicrographs (in cross-polarized light) of the granitoids, with (a) showing the contact of a finer-grained MME (FJS14-06MME) with the host granodiorite (FJS14-06host); (b)–(e) showing the mineralogy and textures of the granite samples (FJS14-06host, FJS14-17host, FJS14-01, and FJS14-22); and (f) showing the arfvedsonite in the Kuiqi alkali feldspar granite (FJS14-15) with the composition (electron-microprobe analysis) of SiO₂ = 51.65 wt.%, Ti₂O = 0.12 wt.%, Al₂O₃ = 0.26 wt.%, Fe₂O₃ = 31.13 wt.%, MnO₂ = 0.28 wt.%, MgO = 0.00 wt.%, CaO = 0.11 wt.%, Na₂O = 12.53 wt.%, and K₂O = 0.00 wt.%. Amp: amphibole; Ap: apatite; Arf: arfvedsonite; Bt: biotite; Mic: muscovite; Pl: plagioclase; Qz: quartz [Colour figure can be viewed at wileyonlinelibrary.com]

precisions better than 1% for most elements except for TiO_2 (~1.5%) and P_2O_5 (~2.0%; Song et al., 2010). Loss on ignition (LOI) analysis was measured by placing 0.9- to 1.1-g sample in the furnace at 1000°C for 4–5 hr before being cooled in a desiccator and reweighted.

The whole-rock major element compositions of FJS14-06MME were analysed at OLMD using an Agilent 5100a ICP-OES instrument. Fifty milligrams of dry rock powder was weighed and fused using 5 times flux sodium metaborate in a platinum crucible. The platinum crucible was placed in the muffle furnace at 1050°C for 60 min before being heated on the Bunsen burner. The molten sample was then poured quickly into a beaker with 5% HNO_3 . Finally, the sample solution was diluted to ~100 g in a polyethylene bottle for analysis. Precisions for all major elements based on rock standards STM-2, RGM-2, and W-2 are better than 2%.

Trace element analysis was done using an Agilent 7900 ICP-MS at OLMD. We digested/dissolved 50-mg rock powder with 1-ml Lefort aqua regia solution and 0.5-ml HF in a Teflon beaker and then placed the beaker with the resulting solution with a high-pressure metal “bomb” in an oven at 190°C for 15 hr. After cooling down, the beaker was kept open on a hotplate at 130°C to incipient dryness before 1-ml HNO_3 was added, and then, the mixture was evaporated to incipient dryness. This was followed by adding 1-ml HNO_3 and 4 ml of ultra-pure water in the same

beaker to be redissolved using the bomb for 2 hr. Finally, the sample solution was diluted to 100 g with 2% HNO_3 in a polyethylene bottle for analysis (Chen et al., 2017). The analytical precision was better than 5%, and the accuracy was generally better than 10% for all elements but Be (12%).

3.3 | Mineral compositions

We chose plagioclase with concentric zoning for major element analysis in the laboratory of Langfang Institute of Regional Geological Survey using a JEOL EPMA-8230 electron-microprobe (EMP) with a beam size of 5- μm diameter, at 15-kV and 20- μA beam current.

3.4 | Whole-rock Sr-Nd-Hf isotopes

The whole-rock Sr-Nd-Hf isotopic compositions were analysed using a Nu Plasma HR multi-collector inductively coupled plasma mass spectrometry (MC-ICP-MS) system in the Radiogenic Isotope Facility at the University of Queensland (RIF-UQ), Australia with sample preparation and analytical details given in Guo et al. (2014). The measured $^{87}\text{Sr}/^{86}\text{Sr}$, $^{143}\text{Nd}/^{144}\text{Nd}$, and $^{176}\text{Hf}/^{177}\text{Hf}$ ratios were corrected for mass fractionation using the exponential law by normalizing to ^{86}Sr /

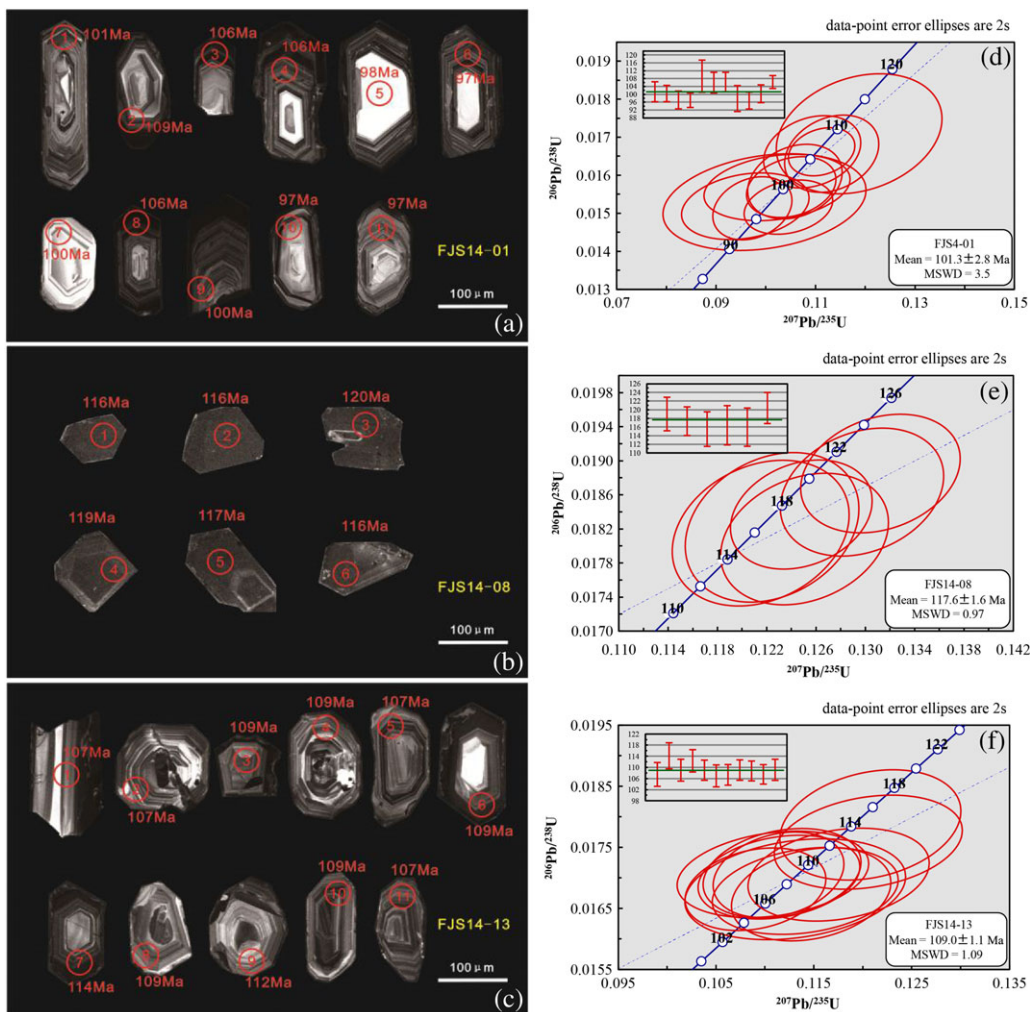


FIGURE 3 Cathodoluminescence (CL) images of zircon grains with LA-ICP-MS U-Pb dating spots as indicated and the Concordia diagrams for samples (a and d) FJS14-01, (b and e) FJS14-08, and (c and f) FJS14-13 [Colour figure can be viewed at wileyonlinelibrary.com]

$^{88}\text{Sr} = 0.1194$, $^{146}\text{Nd}/^{144}\text{Nd} = 0.7219$, and $^{179}\text{Hf}/^{177}\text{Hf} = 0.7325$, respectively. The measured average value for the NBS-987 Sr standard was $^{87}\text{Sr}/^{86}\text{Sr} = 0.710249 \pm 17$ ($n = 23, 2\sigma$). The Nd metal 50 ppb, an in-house Nd standard, had an average $^{143}\text{Nd}/^{144}\text{Nd}$ of 0.511966 ± 6 ($n = 21, 2\sigma$). The repeated measurement of the Hf standard (40 ppb) gave an average $^{176}\text{Hf}/^{177}\text{Hf}$ value of 0.282145 ± 6 ($n = 14, 2\sigma$). The Geological Survey of Japan (GSJ) rock reference sample JG-3 and the U.S. Geological Survey (USGS) rock standard BCR-2 were repeatedly measured along with our samples. Repeated analysis of JG-3 along with our samples gave $^{87}\text{Sr}/^{86}\text{Sr} = 0.705379 \pm 16$ ($n = 2, 2\sigma$), $^{143}\text{Nd}/^{144}\text{Nd} = 0.512612 \pm 7$ ($n = 2, 2\sigma$), and $^{176}\text{Hf}/^{177}\text{Hf} = 0.282883 \pm 5$ ($n = 2, 2\sigma$). Repeated analysis of BCR-2 run along with our samples gave $^{87}\text{Sr}/^{86}\text{Sr} = 0.705022 \pm 13$ ($n = 2, 2\sigma$), $^{143}\text{Nd}/^{144}\text{Nd} = 0.512627 \pm 6$ ($n = 2, 2\sigma$), and $^{176}\text{Hf}/^{177}\text{Hf} = 0.282866 \pm 6$ ($n = 2, 2\sigma$). The JG-3 and BCR-2 run with our samples gave values consistent with the reference values (GeoReM, <http://georem.mpch-mainz.gwdg.de/>; González-Guzmán, Weber, Manjarrez-Juárez, Hecht, & Solari, 2014).

4 | RESULTS

4.1 | Zircon U-Pb ages

Zircon U-Pb age data for the Zhao'an (FJS14-01), Xiamen (FJS14-08), and Putian (FJS14-13) plutons are given in Table A1 and presented in Figures 3a–f. All zircons are colourless, transparent, and columnar grains. The CL images show that they are mostly euhedral and 70–200 μm long with length/width ratio of 1:1–4:1. They have the characteristics of magmatic

zircons with oscillatory zoning (Figures 3a–c). Zircons from the Zhaoan pluton (FJS14-01) have varying Th and U with a Th/U ratio of 0.19–1.01 (Table A1) and give a weighted mean $^{206}\text{Pb}/^{238}\text{U}$ age of 101.3 ± 2.8 Ma ($n = 11$, MSWD = 3.5; Figure 3d), representing the crystallization age of the Zhaoan pluton. Zircons from the Xiamen pluton (FJS14-08) have relatively high Th and U with a Th/U ratio of 0.54–0.79 (Table A1) and give a weighted mean $^{206}\text{Pb}/^{238}\text{U}$ age of 117.6 ± 1.6 Ma ($n = 6$; MSWD = 0.97; Figure 3e) after rejecting the discordant data. This age is similar to the age of 114.8 ± 1.8 Ma in the literature (Yang et al., 2018). Zircons from the Putian pluton (FJS14-13) also have varying Th and U, with a Th/U ratio of 0.69–2.63 (Table A1) and give a weighted mean $^{206}\text{Pb}/^{238}\text{U}$ age of 109.0 ± 1.1 Ma ($n = 11$, MSWD = 1.09; Figure 3f).

Our zircon U-Pb ages and the zircon U-Pb ages from the literature (Table A2) indicate that the magmatism occurred at 119–118 Ma (2 samples), 111–108 Ma (3 samples), and 103–92 Ma (11 samples). In fact, these zircon U-Pb ages on the selected samples are consistent with the whole-rock Rb/Sr isochron age of 100 ± 2 Ma, representing the mean emplacement age of these granitoid plutons (see Figure 7g).

4.2 | Major and trace elements

Whole-rock major and trace element data are given in Tables A3 and A4. The granitoids show a large compositional variation that is to a first-order consistent with varying extents of magma evolution as shown by a large SiO_2/MgO range (17–2,082; Figure 4). With the increase of SiO_2/MgO ratio, the granitoids are progressively more evolved and can be divided into three groups for the convenience of

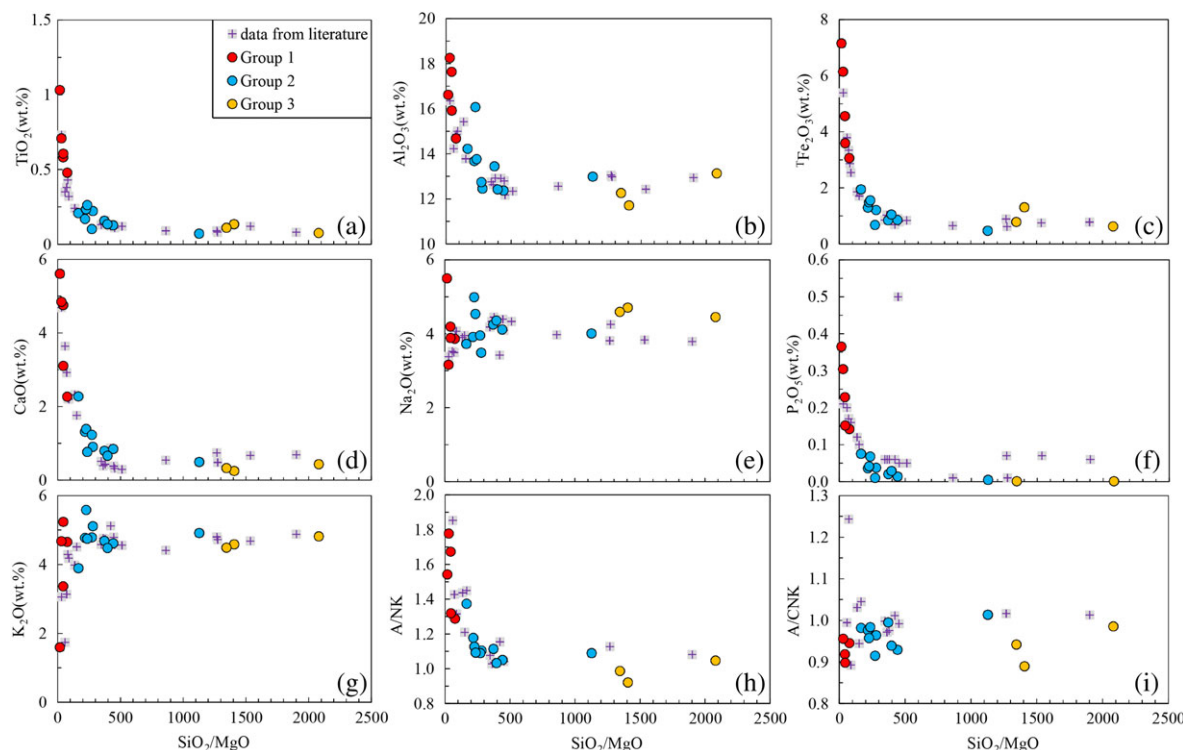


FIGURE 4 SiO_2/MgO variation diagrams of (a) TiO_2 , (b) Al_2O_3 , (c) FeO , (d) CaO , (e) Na_2O , (f) P_2O_5 (g) K_2O , (h) A/NK, and (i) A/CNK molar for our studied samples. Because MgO is positively and SiO_2 is inversely related to the liquidus temperature, using the combined parameter of SiO_2/MgO can magnify and effectively illustrate the effect of varying extent of magma evolution on bulk-rock major and trace elements. The literature data are given in Table A7 [Colour figure can be viewed at wileyonlinelibrary.com]

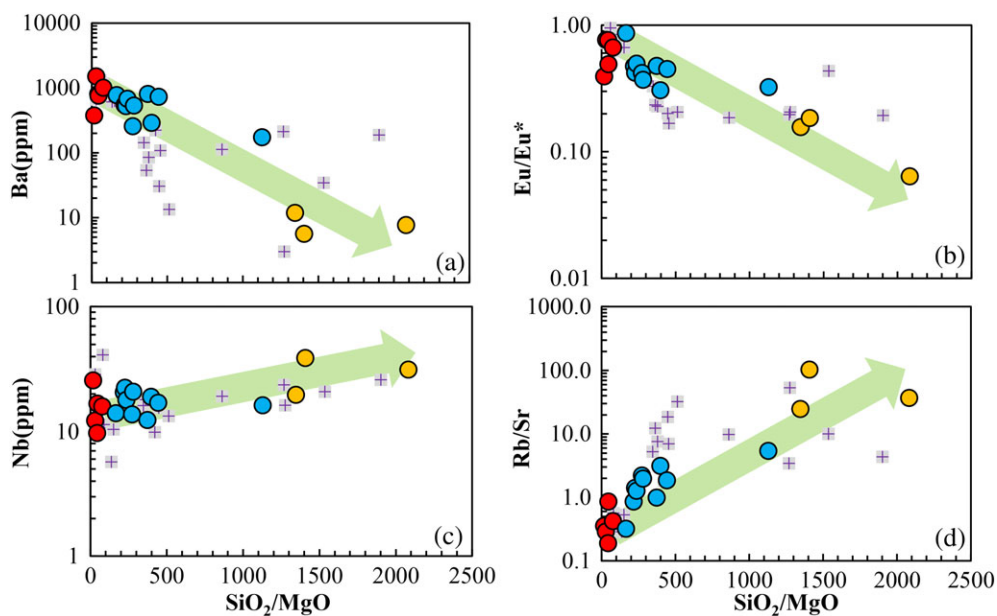


FIGURE 5 SiO_2/MgO variation diagrams of (a) Ba, (b) Eu/Eu^* , (c) Nb, and (d) Rb/Sr. Sample symbols are the same as in Figure 4. The literature data are given in Table A8 [Colour figure can be viewed at wileyonlinelibrary.com]

discussion (Figure 4). This grouping also applies to the abundances and ratios of incompatible trace elements (Figure 5; Tables A4 and A8).

Group 1 samples (from Gunong, Changtai, and Danyang plutons with the lowest SiO_2/MgO of 17–45) are mainly granodiorites, dated from 100 to 97 Ma. They have the highest TiO_2 , Al_2O_3 , Fe_{2O_3} , CaO , P_2O_5 , and A/NK (Figure 4; Tables A3 and A7). These granitoids are enriched in large-ion lithosphere elements (LILEs; e.g., Rb, Th, U, and Pb) and depleted in high-field-strength elements (HFSEs; e.g., Nb, Ta, Ti, and Zr) and show weak negative Ba and Sr anomalies and varying $(\text{La/Yb})_N$ of 7.39–22.71 (Table A4). The LREE fractionation is pronounced with high $(\text{La/Sm})_N$ of 3.31–5.67, whereas the HREEs are relatively flat with $(\text{Gd/Yb})_N = 1.51\text{--}2.23$ (Table A4). Group 1 samples have weak negative Eu anomalies (Figure 5b; Table A4; $\text{Eu}/\text{Eu}^* = 0.39\text{--}0.76$; $\text{Eu}/\text{Eu}^* = 2\text{Eu}_N/(\text{Sm}_N + \text{Gd}_N)$, where the subscript N refers to chondrite-normalized value). Both the host and MME show a similar magnitude of negative Eu anomalies.

Group 2 samples (from Zhao'an, Huxi, Changqiao, Xiamen, Huacuo, Weitou, Quanzhou, Putian, Dacenshan, and Nanzhen plutons with a high SiO_2/MgO of 166–1,128) are biotite granite, biotite monzogranite, and monzogranite, dated from 119 to 93 Ma. They have lower TiO_2 , Al_2O_3 , Fe_{2O_3} , CaO , P_2O_5 , and A/NK than Group 1 (Figure 4; Table A3). These granitoids are more enriched in LILEs (e.g., Rb, Th, U, and Pb), depleted in HFSEs (e.g., Nb, Ta, Ti, and Zr), and show moderate Ba and negative Sr anomalies with varying $(\text{La/Yb})_N$ ratios of 5.49–15.72 (Table A4). The LREE fractionation is pronounced with $(\text{La/Sm})_N = 3.43\text{--}7.33$, whereas the HREEs are relatively flat with $(\text{Gd/Yb})_N = 0.93\text{--}2.43$. They have negative Eu anomalies (Figure 5b; Table A4; $\text{Eu}/\text{Eu}^* = 0.31\text{--}0.87$).

Group 3 samples (from Chengxi, Kuiqi, and Sansha plutons with SiO_2/MgO of 1,345–2,082) are highly evolved alkali feldspar granites, dated from 101 to 92 Ma. They thus have extremely high SiO_2/MgO and low CaO with similar levels of TiO_2 , Al_2O_3 , and Fe_{2O_3} to Group 2 samples (Figure 4; Table A3). Their extreme enrichment in LILEs (e.g., Rb, Th, U, and Pb), depletion in HFSEs (e.g., Nb, Ta, Ti, and Zr), and strong negative Ba and Sr anomalies (Table A4; $\text{Eu}/\text{Eu}^* = 0.06\text{--}0.19$)

are expected as the result of advanced extents of fractionation, which is also consistent with the varying $(\text{La/Yb})_N$ (2.84–7.10), $(\text{La/Sm})_N$ (2.91–6.61), and $(\text{Gd/Yb})_N$ (1.04–1.47) ratios (Table A4).

Therefore, with increasing SiO_2/MgO , samples from Group 1 to Group 3 are progressively more evolved with decreasing TiO_2 , Al_2O_3 , Fe_{2O_3} , CaO , P_2O_5 , A/NK ratio (Figure 4), Ba, and Eu/Eu^* ratio (Figure 5b) and increasing Nb and Rb/Sr ratio (Figures 5c–d). The three groups are all relatively depleted in HFSEs with overlapping REE ratios (Figure A1). They have a similar A/CNK ratio but varying A/NK values with Group 1 > Group 2 > Group 3, which is consistent with the progressive removal of Al_2O_3 and CaO because of Ca-rich plagioclase fractionation (Figure 4).

4.3 | Plagioclase compositions

The data are given in Table A5. Plagioclase from two granodiorite host–MME pairs (FJS14-06host–MME; FJS14-17host–MME) was analysed to understand the significance of the MMEs in the context of the granitoid petrogenesis. Plagioclase in the MME from the Changtai pluton (FJS14-06) has $\text{An}_{40\text{--}55}$ (Figure 6a), which is much higher than that in the granodiorite host with $\text{An}_{25\text{--}39}$ (Figure 6b). Plagioclase in the MME from the Danyang pluton (FJS14-17; Figure 6c; $\text{An} = 33\text{--}47$) is similar to or more calcic than that in the granodiorite host (Figure 6d; $\text{An} = 23\text{--}41$).

4.4 | Whole-rock Sr–Nd–Hf isotopes

Whole-rock Sr–Nd–Hf isotopic compositions are given in Table A6. The correlated Nd ($\epsilon\text{Nd}_{(t)} = -6.09$ to -1.158) and Hf ($\epsilon\text{Hf}_{(t)} = -4.68$ to $+3.35$) isotopic variation reflects parental magma compositional differences as the result of varying sources and processes of the granitoids. The observed large Sr isotopic variation ($^{87}\text{Sr}/^{86}\text{Sr} = 0.7068$ to 1.311) is consistent with the large Rb/Sr ratio variation among samples (Figure 5d; Shao, Niu, Regelous, & Zhu, 2015; Wu et al., 2007) and

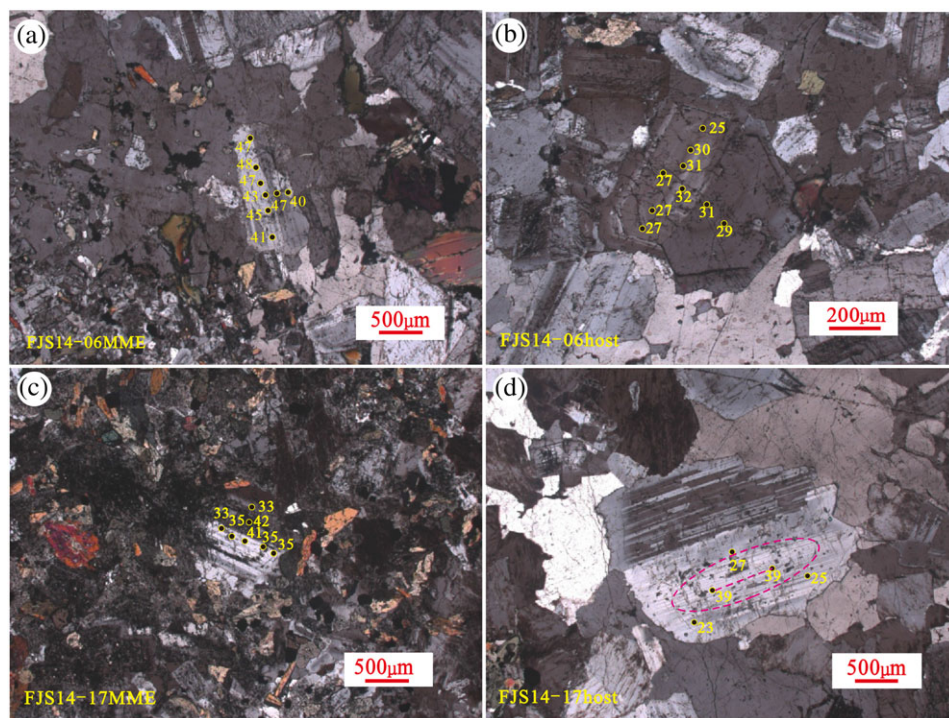


FIGURE 6 Photomicrographs (in cross-polarized light) showing small compositional variation (in terms of the An value defined as Ca/(Ca + Na); electron probe analysis) of selected plagioclase crystals in representative samples as indicated (samples FJS14-06MME, FJS14-06host, FJS14-17MME, and FJS14-17host, respectively, in panels [a–d], respectively) [Colour figure can be viewed at wileyonlinelibrary.com]

gives a significant (>99% confidence level) isochron age of 100 ± 2 Ma (Figure 7g), representing the mean emplacement age of the granitoids.

5 | DISCUSSION

5.1 | Temporal-spatial distribution

Zhou and Li (2000) reported that the granitoids are progressively younger from the interior towards the south-east coast of continental China. However, Li and Li (2007) argued that the temporal-spatial distribution of the magmatism is more complex. Sun (2006) and Zhou et al. (2006) showed that the Cretaceous granites are distributed in a very large area of the Cathaysia Block, which is ~1,000 km long and 500 km wide, rather than liner distribution along the coastline. More recently, Niu et al. (2015) demonstrated that in eastern continental China, the Jurassic–Cretaceous (ca. 190 to ca. 90 Ma) granitoids are distributed randomly in space and time in a wide zone in excess of >1,000 km. Such granitoid distributions in space and time are best explained as a special consequence of plate tectonics, genetically associated with the paleo-Pacific Plate subduction beneath eastern continental China (Niu, 2005, 2014). Specifically, the dehydration of the paleo-Pacific Plate stagnant horizontally in the mantle transition zone beneath eastern continental China ultimately caused the lithosphere thinning and basaltic magmatism. Underplating and intrusion of such basaltic magmas indirectly caused the crustal melting and the widespread granitoid magmatism in the interiors of eastern continental China (i.e., “intra-plate” granitoid magmatism; Niu et al., 2015).

The youngest granitoids along the coastal region of south-east continental China of ca. 90 Ma indicate the cessation of the paleo-Pacific

Plate subduction at this time or slightly earlier at ca. 100 Ma, caused by the trench jam upon the arrival of a microcontinent (the present-day Chinese continental shelf basement; Niu et al., 2015). This means that the coastal granitoids represent the last episode of the granitoid magmatism in response to the paleo-Pacific Plate subduction in the Cretaceous (Niu et al., 2015). This understanding leads to the hypothesis that the coastal granitoids are immediately “subduction” related and differ from those “intra-plate” granitoids in the interiors of eastern continental China. Indeed, the coastal granitoids we report here have significantly greater mantle input than the “intra-plate” granitoids (Hong et al., 2018).

5.2 | Petrogenesis

5.2.1 | Host and MMEs

Samples FJS14-06host and FJS14-06MME of the Changtai pluton have similar $^{87}\text{Sr}/^{86}\text{Sr}_{(i)}$ (0.705961; 0.705928), $\epsilon\text{Nd}_{(t)}$ (-3.24; -3.29), and $\epsilon\text{Hf}_{(t)}$ (-0.92; -0.55) isotopic ratios (Table A6; Figures 7a–d), indicating that they share the same parental magma (Chen et al., 2016; Chen et al., 2017). Their small differences in major and trace element abundances are controlled by the model mineralogy with the MMEs having greater modal amphiboles crystallized at early stage of the same system. This is also consistent with the MMEs having higher plagioclase An than that of the host (Table A5).

5.2.2 | Genetic relationship between the coastal granitoids

Although previous studies agreed that the petrogenesis of the coastal granitoids involved significant crustal material, different views exist, including that (a) the granitoids were formed by different degrees of

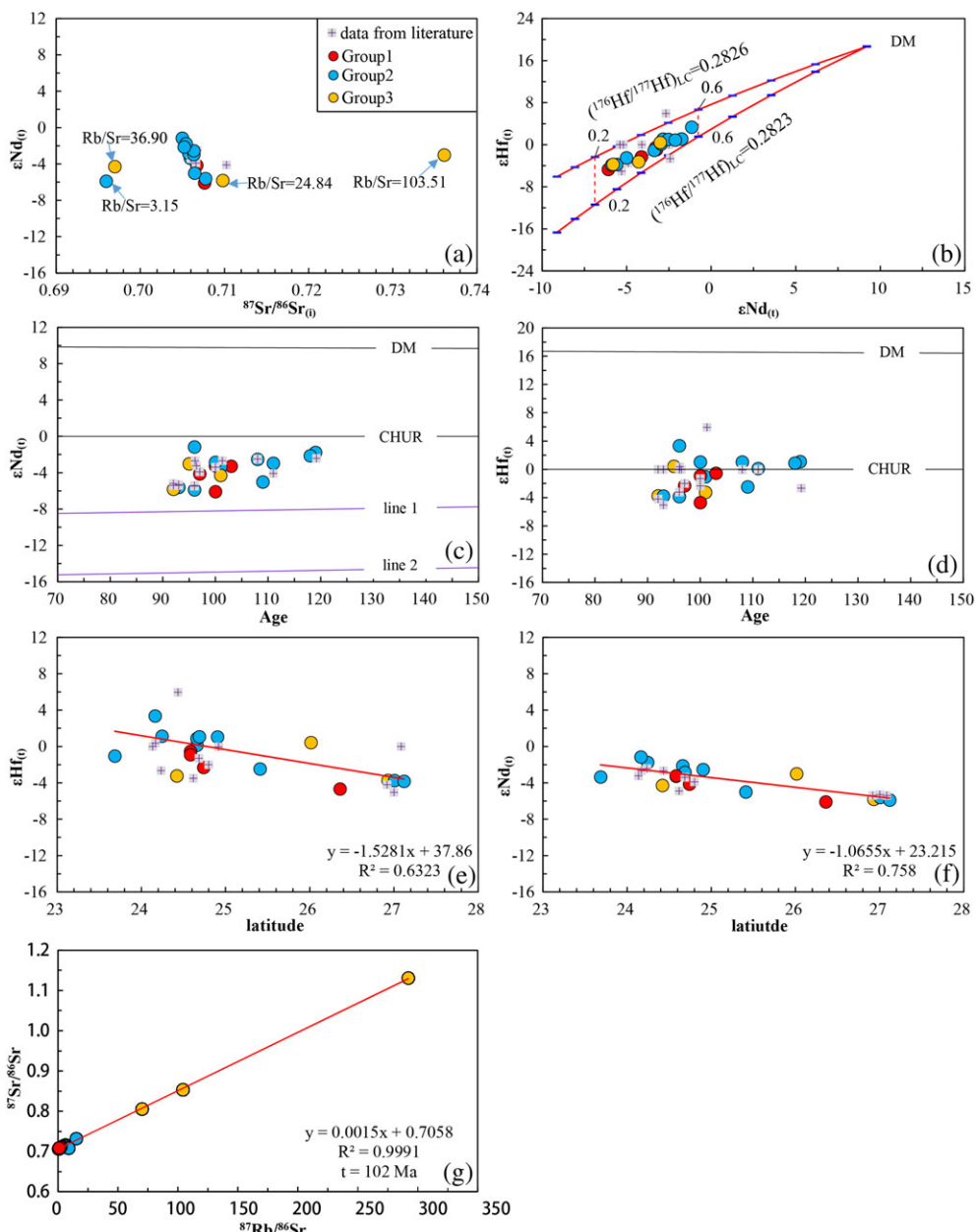


FIGURE 7 Sr-Nd-Hf isotope data: (a) $^{87}\text{Sr}/^{86}\text{Sr}_{(i)}$ versus $\epsilon_{\text{Nd}}(t)$; (b) $\epsilon_{\text{Nd}}(t)$ versus $\epsilon_{\text{Hf}}(t)$; (c and d) age versus $\epsilon_{\text{Nd}}(t)$ and $\epsilon_{\text{Hf}}(t)$, respectively; (e and f) correlation of $\epsilon_{\text{Hf}}(t)$ and $\epsilon_{\text{Nd}}(t)$ as a function of latitude; and (g) Rb-Sr isochron of our samples. The data used to calculate the $^{87}\text{Sr}/^{86}\text{Sr}_{(i)}$, $\epsilon_{\text{Hf}}(t)$, $\epsilon_{\text{Nd}}(t)$, and the reference line of the depleted-mantle (DM) are given in Table A6. Binary isotope mixing calculations of (b) used the DM data from Salters and Stracke (2004) and the lower continental crust data from Rudnick and Gao (2003) and Shen, Zhu, Liu, Xu, and Ling (1993). The data of line 1 and line 2 in (c) are from Shen et al. (1993). Sample symbols are the same as in Figure 4. The literature data are given in Table A9 [Colour figure can be viewed at wileyonlinelibrary.com]

fractional crystallization of magmas produced by crust–mantle interaction (Qiu et al., 2004; Qiu et al., 2008); (b) these granitoids were crystallized from magmas formed by the partial melting of prior tonalitic to granodioritic rocks (Zhao, Qiu, Liu, & Wang, 2015); and (c) mantle-derived mafic magmas mixed with crust-derived magmas (Zhao et al., 2016). However, most of these previous studies focused on single plutons or composite granitoid complexes without along-coast regional comparison.

The overlapping zircon U-Pb ages (Figure 3) and Nd and Hf isotopic compositions (Figure 7) suggest that the three groups of granites must have been produced in the same time frame and share similar sources and processes in terms of their parental magma generation.

The high SiO_2/MgO (Figures 4 and 5), high Rb/Sr (Figure 5d), and low Ba and Eu/Eu^{*} of the Group 3 samples are consistent with their being highly evolved products of a similar magmatic lineage (Figures 4 and 5).

The correlated Nd ($\epsilon_{\text{Nd}}(t) = -6.1$ to -1.2) and Hf ($\epsilon_{\text{Hf}}(t) = -4.7$ to $+3.4$) isotopic variations (Figure 7b) between samples reflect their parental magma compositional differences inherited from varying sources and processes. Figure 7c-d shows that there is mantle contribution to the granitoids, a scenario that has long been recognized (Deng et al., 2016; Li et al., 2014; Li & Li, 2007; Li, Qiu, & Xu, 2012; Zhou & Li, 2000). The best interpretation is that these granitoids result from melting of mature crustal material (lower Nd–Hf isotopes) triggered by mantle-derived melts (higher Nd–Hf isotopes) that

contributed both heat and materials. Furthermore, a simple mixing calculation suggests ~20–60% mantle contribution to the petrogenesis of these granitoids in terms of Nd–Hf isotopes (Figure 7b; Table A6).

5.2.3 | The cause of the large SiO_2/MgO range

We stated above that the large SiO_2/MgO range of these granitoid plutons represented by our samples resulted from varying extent of fractional crystallization from their respective parental magmas (Figures 4 and 5). To quantify this interpretation, we applied the Rhyolite-MELTS (Gualda, Ghiorso, Lemons, & Carley, 2012) to model the crystallization processes. We used the composition of the Group 1 sample (FJS14-06host) with the lowest SiO_2/MgO and 6 wt.% H_2O to approximate the primitive parental magmas. The calculation was done at 3 kbar. The mineralogy chosen in the calculation was based on the petrography. The results explain the data as expected in terms of the SiO_2/MgO ratio (Figures 4 and 5). Relative to the Group 1 sample (FJS14-06host), the extents of fractional crystallization of the Group 2 and Group 3 samples were ~24–51% and ~51–67%, respectively (Figure 8a). In Figure 8b, all samples display progressive fractional crystallization dominated by plagioclase and K-feldspar with the Group 3 samples having the highest extent of fractional crystallization (Figures 4 and 8a).

In summary, the parental magmas of these granitoids were derived from crustal melting induced by mantle-derived melts equivalent to ~20–60% mantle contribution in terms of Nd–Hf isotopes (Figure 7b). The varying extent of fractional crystallization of such parental magmas,

as manifested by the varying SiO_2/MgO ratios of the three groups of granitoid samples (Figures 4, 5, and 8), formed these coastal granitoids.

5.2.4 | The classification of the granitoids

This is not the focus of the paper, but the discussion is necessary here. In studying the petrogenesis of granites and granitoids, it is common that researchers classify the rocks into M-type, I-type, S-type, and A-type granite/granitoids (Chappell & White, 1992; Pitcher, 1983; Whalen, Currie, & Chappell, 1987). Such classification has also been emphasized in studying the Cretaceous granitoids along the south-east coast of continental China in the past 20 years (Li et al., 2007; Li, Qiu, Jiang, Xu, & Hu, 2009; Liu et al., 2012; Qiu et al., 2008; Wu et al., 2003; Xiao et al., 2007). However, we show that such classification or “discrimination” diagrams have no significance at least for the granitoids that we studied along the south-east coast of continental China. This is because the tectonic setting of these granitoids is known and tectonically well-constrained (see above and below), but if we were indiscriminately applying such classification, we would be both misled and misleading in terms of tectonic settings. For example, it is clear from the SiO_2/MgO variation diagrams (Figures 4 and 5) that our granitoid samples represent varying degrees of magma evolution (dominantly fractional crystallization) from spatially and temporally similar parental magmas, rather than genetically different S-, I-, and A-types or fractionated (FG) or unfractionated (OGT) types of granitoids as shown in Figure 9.

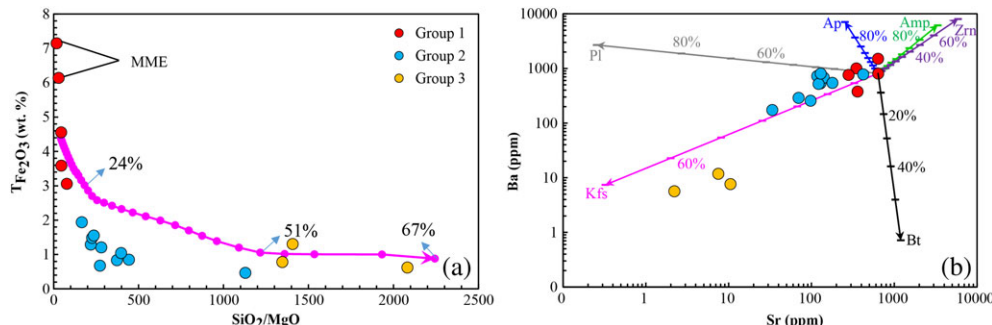


FIGURE 8 (a) Fe_2O_3 versus SiO_2/MgO (wt.% on anhydrous basis). The pink line represents rhyolite-MELTS fractional crystallization modelling by assuming the most primitive Group 1 sample (FJS14-06host) as the parental granitoid liquid composition with water content of 6 wt.% at 3 kbar. The arrow indicates that the residual melt fraction decreases as temperature falls as a function of the increasing percentage (%) of crystallization. (b) Ba versus Sr covariation, indicating that the sample compositional variation is largely caused by alkali feldspar fractionation. The trend lines of fractional crystallization of minerals (Ap: apatite; Bt: biotite; Kfs: K-feldspar; Pl: plagioclase; and Zrn: zircon) were calculated using the data from <https://earthref.org/GEM/>. Sample symbols are the same as in Figure 4 [Colour figure can be viewed at wileyonlinelibrary.com]

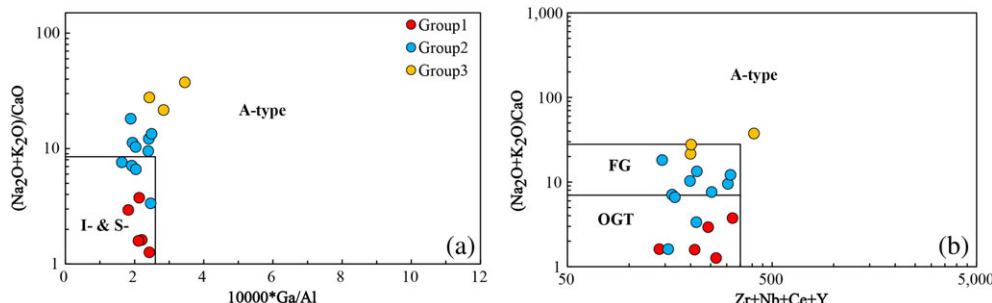


FIGURE 9 Granitoid classification diagrams of Whalen et al. (1987): (a) $(\text{Na}_2\text{O} + \text{K}_2\text{O})/\text{CaO}$ versus $10,000 * \text{Ga}/\text{Al}$ and (b) $(\text{Zr} + \text{Nb} + \text{Ce} + \text{Y})$ versus $(\text{Na}_2\text{O} + \text{K}_2\text{O})/\text{CaO}$. Sample symbols are the same as in Figure 4. FG: fractionated felsic granites; OGT: unfractionated M-, I-, and S-type granites [Colour figure can be viewed at wileyonlinelibrary.com]

5.3 | Geological background

Zhou and Li (2000) proposed that the subducting slab of the paleo-Pacific Plate steepened (slab rollback) during 180–80 Ma, and varying degrees of mantle wedge melting produced basaltic magmas. These basaltic magmas rose and heated the lower continental crust to produce the felsic magmas parental to the granitoids in the region. Li and Li (2007) proposed a flat-slab subduction model to explain the formation of the ~1,300 km wide intracontinental orogen during 265–190 Ma and used the flat-slab break-off model to explain the 190–80 Ma South China granitoid petrogenesis. The appearance of the A-type granite (190 Ma) in southern Jiangxi Province would suggest a tectonic setting change. Li and Li (2007) suggested that the trend of granitoids becoming younger towards the coast after 150 Ma was caused by the break-up of the flat subducting slab. Niu (2005, 2014) and Niu et al. (2015) suggested that the Mesozoic granitoids throughout eastern continental China have connection with the lithospheric thinning in eastern China and resulted from “basal hydration weakening” caused by dehydration of the subducted slab lying in the mantle transition zone.

Compared with the coeval granitoids in the vast interiors of eastern continental China, or the “intra-plate” granitoids, which are genetically and ultimately associated with the mantle transition zone paleo-Pacific slab dehydration, lithosphere thinning, and basaltic magmatism (Niu, 2014; Niu et al., 2015), the granitoids we studied along the south-east coastline of continental China are directly caused by paleo-Pacific Plate subduction, although the detailed history of such subduction remains controversial (Deng et al., 2016; Li, 2000; Li et al., 2012; Li et al., 2014; Li & Li, 2007; Li, Zhou, Chen, Wang, & Xiao, 2011; Lin, Cheng, Zhang, & Wang, 2011; Mao, Li, & Wang, 1998; Niu, 2014; Shan et al., 2014; Wu, Dong, Wu, Zhang, & Ernst, 2017; Zhao et al., 2015; Zhao, Hu, Zhou, & Liu, 2007). With all the observations and above discussions considered, we propose that the granitoids in the present study represent the last episode of magmatism associated with the paleo-Pacific Plate subduction beneath continental China at the time of, or shortly before, the trench jam and cessation of the subduction, whose locus is marked by the arc-shaped south-east coastline of continental China (Niu et al., 2015). This scenario can be readily explained by the subducting slab dehydration-induced mantle wedge melting and basaltic magma generation (Figure 10a). The basaltic magmas produced in this way ascend and underplate/intrude of the mature crust, contributing both heat and material for crustal melting and granitoid magma generation, which is also consistent with both mantle and crustal contributions indicated by the Nd–Hf isotopes (Figure 7). These results confirm previous interpretation (Chen et al., 2013; Qiu et al., 2008; Qiu, Li, Liu, & Zhao, 2012) and offer a general solution to the petrogenesis of all the Cretaceous granitoids along the south-east coast of the continental China.

An important new observation is that the granitoids show a northward $\epsilon_{\text{Nd}_{\text{t}}}$ and $\epsilon_{\text{Hf}_{\text{t}}}$ (Figure 7e,f) isotopic decrease, which may be caused by several possibilities, as one travels northward, as follows: (a) There are more terrigenous sediments that contributed to the mantle wedge for the basaltic magmatism in the first place, (b) there are compositional differences of the existing crust, and (c) there is increasing crustal thickness for higher extent of crustal assimilation. With all factors considered, the best interpretation is the northward crustal thickening, permitting a greater extent of crustal assimilation (Figure 10b).

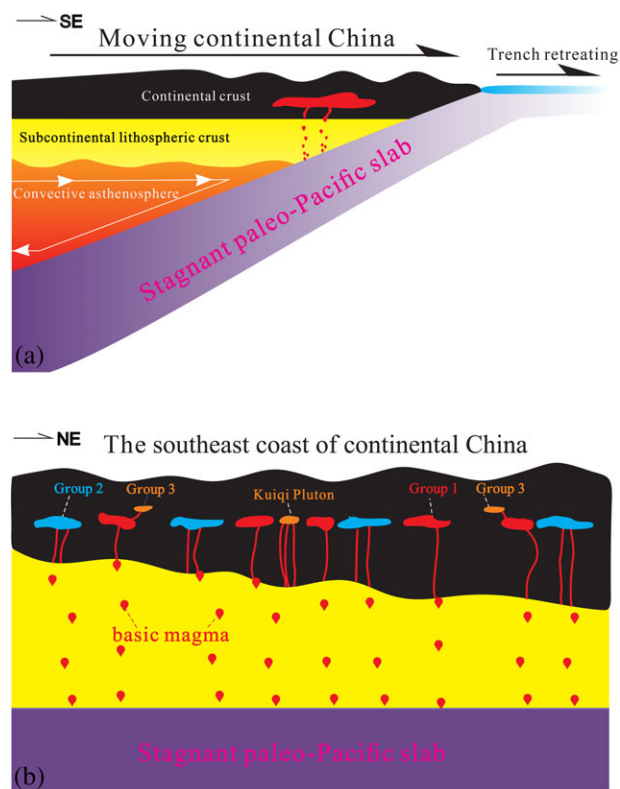


FIGURE 10 (a) Conceptual model of the Cretaceous magmatism in a NW-SE cross-section, which is roughly perpendicular to the coastline and is interpreted to be consistent with the paleo-Pacific Plate subduction (Niu et al., 2015). (b) Conceptual model of the SW-NE direction Cretaceous magmatism along the south-east coastline of continental China [Colour figure can be viewed at wileyonlinelibrary.com]

6 | CONCLUSIONS

- (1) We report for the first time the zircon U-Pb ages for the Zhaohan (101 ± 3 Ma) and Putian (109 ± 1 Ma) plutons (Figure 3). The zircon U-Pb age of the Xiamen pluton (118 ± 2 Ma) agrees with the age data in the literature. These age data on selected granitoid samples and the whole-rock Rb-Sr isochron age of 100 ± 2 Ma (Figure 7) on all of the studied plutons together place constraints on the coastal granitoids representing the last episode of the magmatism associated with the paleo-Pacific Plate subduction, with the magmatism ending because of the subduction cessation at ca. 100 Ma.
- (2) The origin of the magmas parental to these granitoids is best understood as resulting from paleo-Pacific slab subducting-induced mantle wedge melting, whose basaltic melt intruded/underplated the crust for the crustal melting and granitoid production (Figure 10). This is manifested by both mantle (20–60%) and crustal (40–80%) contributions to the granitoids in terms of Nd–Hf isotope compositions (Figure 7b).
- (3) A varying extent of fractional crystallization dominated magma evolution resulted in the observed compositional diversity of these granitoids as expressed in the SiO_2/MgO variation diagrams (Figures 4 and 5). Rhyolite-MELTS modelling suggests that relative to Group 1 samples (FJS14-06host), the extent of fractional crystallization of Group 2 and Group 3 samples was ~24–51% and ~51–64%, respectively (Figure 8a). Group 2 samples displayed a progressive fractional

- crystallization of plagioclase and orthoclase, and Group 3 samples showed further fractional crystallization dominated by orthoclase.
- (4) The northward $\epsilon\text{Nd}_{(t)}$ and $\epsilon\text{Hf}_{(t)}$ decrease is best explained as northward crustal thickening (Figures 7e-f), which permits enhanced crustal magma assimilation.
 - (5) The widely used classification or finger-printing geochemical diagrams for granitoids (Figure 9) have no significance, at least for the granitoids that we studied.

ACKNOWLEDGEMENTS

We thank Li Jiyong, Shao Fengli, and Ye Lei for the fieldwork assistance and Qin Hong and Su Li for the assistance in major and trace element analysis. This work was supported by the National Natural Science Foundation of China (NSFC41630968, 41130314, and 41776067), the Chinese Academy of Sciences (Innovation Grant Y42217101L), the Scientific and Technological Innovation Project financially supported by Qingdao National Laboratory for Marine Science and Technology (2015ASKJ03), the NSFC-Shandong Joint Fund for Marine Science Research Centers (U1606401), and the 111 Project (B18048).

ORCID

Qiqi Xue  <https://orcid.org/0000-0002-2789-3545>

REFERENCES

- Blichert-Toft, J., & Albarède, F. (1997). The Lu-Hf geochemistry of chondrites and the evolution of the mantle-crust system. *Earth Planet Sci Lett*, 148, 243–258. Erratum. *Earth Planet. Sci. Lett.* 154, (1998) 349.
- Chappell, B. W., & White, A. J. R. (1992). I- and S-type granites in the Lachlan Fold Belt. *Geological Society of America Special Papers*, 272, 1–26. <https://doi.org/10.1130/SPE272-p1>
- Chen, C. H., Lu, H. Y., Lin, W., & Lee, C. Y. (2006). Thermal event records in SE China coastal areas: Constraints from Monazite Ages of beach sands from two sides of the Taiwan Strait. *Chemical Geology*, 231, 118–134. <https://doi.org/10.1016/j.chemgeo.2006.01.023>
- Chen, J. Y., Yang, J. H., Zhang, J. H., Sun, J. F., & Wilde, S. A. (2013). Petrogenesis of the Cretaceous Zhangzhou batholith in southeastern China: Zircon U-Pb age and Sr-Nd-Hf-O isotopic evidence. *Lithos*, 162–163, 140–156. <https://doi.org/10.1016/j.lithos.2013.01.003>
- Chen, S., Niu, Y. L., Li, J. Y., Sun, W. L., Zhang, Y., Hu, Y., & Shao, F. L. (2016). Syncollisional adakitic granodiorites formed by fractional crystallization: Insights from their enclosed mafic magmatic enclaves (MMEs) in the Qumushan pluton, North Qilian Orogen at the northern margin of the Tibetan Plateau. *Lithos*, 248/251, 455–468.
- Chen, S., Wang, X. H., Niu, Y. L., Sun, P., Duan, M., Xiao, Y. Y., ... Xue, Q. Q. (2017). Simple and cost-effective methods for precise analysis of trace element abundances in geological materials with ICP-MS. *Science Bulletin*, 62, 277–289. <https://doi.org/10.1016/j.scib.2017.01.004>
- Deng, J. F., Feng, Y. F., Di, Y. J., Liu, C., Xiao, Q. H., Su, S. G., ... Xiong, L. (2016). The intrusive spatial temporal evolutional framework in the Southeast China. *Geological Review*, 62, 3–16. (in Chinese with English abstract).
- González-Guzmán, R., Weber, B., Manjarrez-Juárez, R., Hecht, L., & Solari, L. (2014). Petrogenesis of basement rocks in the southern Chiapas Massif: Implications on the tectonic evolution of the Maya Block. *Goldschmidt*.
- Griffin, W. L., Wang, X., Jackson, S. E., Pearson, N. J., O'Reilly, S. Y., Xu, X., & Zhou, X. M. (2002). Zircon chemistry and magma mixing, SE China: In-situ analysis of Hf isotopes, Tonglu and Pingtan igneous complexes. *Lithos*, 61(3-4), 237–269.
- Gualda, G. A. R., Ghiorso, M. S., Lemons, R. V., & Carley, T. L. (2012). Rhyolite-MELTS: A modified calibration of MELTS optimized for silica-rich, fluidbearing magmatic systems. *Journal of Petrology*, 53, 875–890. <https://doi.org/10.1093/petrology/egr080>
- Guo, P. Y., Niu, Y. L., Ye, L., Liu, J. J., Sun, P., Cui, H. X., ... Feng, Y. X. (2014). Lithosphere thinning beneath west North China Craton: Evidence from geochemical and Sr-Nd-Hf isotope compositions of Jining basalts. *Lithos*, 202/203, 37–54.
- He, Z. Y., Xu, X. S., & Niu, Y. L. (2010). Petrogenesis and tectonic significance of a Mesozoic granite–syenite–gabbro association from inland South China. *Lithos*, 119, 621–641. <https://doi.org/10.1016/j.lithos.2010.08.016>
- Hong, D., Niu, Y. L., Xiao, Y. Y., Sun, P., Kong, J. J., Guo, P. Y., Shao, F. L., ... Chen, S. (2018). Origin of the Jurassic-Cretaceous intraplate granitoids in Eastern China as a consequence of paleo-Pacific plate subduction. *Lithos*, 322, 405–419.
- Li, L. L., Zhou, H. W., Chen, Z. H., Wang, J. R., & Xiao, Y. (2011). Geochemical characteristics of granites in Taimushan area, Fujian Province, and their geological significance. *Acta Petrologica et Mineralogica*, 30, 593–609.
- Li, X. H. (2000). Cretaceous magmatism and lithosphere extension in Southeast China. *Journal of Asian Earth Sciences*, 18, 293–305. [https://doi.org/10.1016/S1367-9120\(99\)00060-7](https://doi.org/10.1016/S1367-9120(99)00060-7)
- Li, X. H., Li, W. X., Wang, X. C., Li, Q. L., Liu, Y., Tang, G. Q., ... Wu, F. Y. (2010). SIMS U-Pb zircon geochronology of porphyry Cu-Au-(Mo) deposits in the Yangtze River Metallogenic Belt, eastern China: Magmatic response to Early Cretaceous lithospheric extension. *Lithos*, 119, 427–438. <https://doi.org/10.1016/j.lithos.2010.07.018>
- Li, X. H., Li, Z. X., Li, W. X., Liu, Y., Yuan, C., Wei, G. J., & Qi, C. S. (2007). U-Pb zircon, geochemical and Sr-Nd-Hf isotopic constraints on age and origin of Jurassic I- and A-type granites from central Guangdong, SE China: A major igneous event in response to foundering of a subducted flat-slab? *Lithos*, 96, 186–204. <https://doi.org/10.1016/j.lithos.2006.09.018>
- Li, Z., Qiu, J. S., Jiang, S. Y., Xu, X. S., & Hu, J. (2009). Petrogenesis of the Jinshan Granitic Composite Pluton in Fujian Province: Constraints from elemental and isotopic geochemistry. *Acta Geologica Sinica*, 83, 515–527.
- Li, Z., Qiu, J. S., & Xu, X. S. (2012). Geochronological, geochemical and Sr-Nd-Hf isotopic constraints on petrogenesis of late Mesozoic gabbro-granite complexes in the southeast coast of Fujian, South China: Insights into a depleted mantle source region and crust-mantle interactions. *Geological Magazine*, 149, 459–482. <https://doi.org/10.1017/S0016756811000793>
- Li, Z., Qiu, J. S., & Yang, X. M. (2014). A review of the geochronology and geochemistry of Late Yanshanian (Cretaceous) plutons along the Fujian coastal area of southeastern China: Implications for magma evolution related to slab break-off and rollback in the Cretaceous. *Earth-Science Reviews*, 128, 232–248. <https://doi.org/10.1016/j.earscirev.2013.09.007>
- Li, Z. X., & Li, X. H. (2007). Formation of the 1300-km-wide intracontinental orogen and postorogenic magmatic province in Mesozoic South China: A flat-slab subduction model. *Geology*, 35, 179–182. <https://doi.org/10.1130/G23193A.1>
- Lin, Q. C., Cheng, X. W., Zhang, Y. Q., & Wang, F. Y. (2011). Evolution of granitoids in the active continental margin: A case study of the Fuzhou compound complex. *Acta Geologica Sinica*, 85, 1128–1133. (in Chinese with English abstract).
- Liu, Q., Yu, J. H., Wang, Q., Su, B., Zhou, M. F., Xu, H., & Cui, X. (2012). Ages and geochemistry of granites in the Pingtan-Dongshan Metamorphic Belt, Coastal South China: New constraints on Late Mesozoic magmatic evolution. *Lithos*, 150, 268–286. <https://doi.org/10.1016/j.lithos.2012.06.031>
- Liu, Y. S., Gao, S., Gao, C. G., Hu, Z. C., Wang, D. B., & Zong, K. Q. (2010). Continental and oceanic crust recycling-induced melt-peridotite interactions in the Trans-North China Orogen: U-Pb dating, Hf isotopes and trace elements in zircons from mantle xenoliths. *Journal of Petrology*, 51, 537–571. <https://doi.org/10.1093/petrology/egp082>
- Ludwig, K. R. (2003). *User's manual for Isoplot 3.00: A geochronological toolkit for Microsoft Excel*. Special Publication 4 (pp. 1–70). Berkeley, CA: Berkeley Geochronology Center.
- Lugmair, G. W., Marti, K. (1978). Lunar initial $^{143}\text{Nd}/^{144}\text{Nd}$: Differential evolution of the lunar crust and mantle. *Earth and Planetary Science Letters*, 39(3):349–357.
- Mao, J. W., Li, H. Y., & Wang, D. H. (1998). Ore-forming of Mesozoic polymetallic deposits in South China and its relationship with mantle plume. *Bulletin of Mineralogy, Petrology and Geochemistry*, 19, 130–132.

- Niu, Y. L. (2005). Generation and evolution of basaltic magmas: Some basic concepts and a hypothesis for the origin of the Mesozoic–Cenozoic volcanism in eastern China. *Geological Journal of China Universities*, 11, 9–46.
- Niu, Y. L. (2014). Geological understanding of plate tectonics: Basic concepts, illustrations, examples and new perspectives. *Global Tectonics and Metallogenesis*, 10, 23–46.
- Niu, Y. L., Liu, Y., Xue, Q. Q., Shao, F. L., Chen, S., Duan, M., ... Zhang, Y. (2015). Exotic origin of the Chinese continental shelf: New insights into the tectonic evolution of the western Pacific and eastern China since the Mesozoic. *Science Bulletin*, 60, 1598–1616. <https://doi.org/10.1007/s11434-015-0891-z>
- Pitcher, W. S. (1983). Granite type and tectonic environment. In K. Hsu (Ed.), *Mountain building processes* (pp. 19–40). London: Academic Press.
- Qiu, J. S., Li, Z., Liu, L., & Zhao, J. L. (2012). Petrogenesis of the Zhangpu composite granite pluton in Fujian province: Constraints from zircon U-Pb ages, elemental geochemistry and Nd-Hf isotopes. *Acta Geologica Sinica*, 86, 561–576. (in Chinese with English abstract).
- Qiu, J. S., Wang, D. Z., McInnes, B. I. A., Jian, S. Y., Wang, R. C., & Kanisawa, S. (2004). Two subgroups of A-type granites in the coastal area of Zhejiang and Fujian Provinces, SE China: Age and geochemical constraints on their petrogenesis. *Transactions of the Royal Society of Edinburgh: Earth Sciences*, 95, 227–236. <https://doi.org/10.1017/S0263593300001036>
- Qiu, J. S., Xiao, E., Hu, J., Xu, X. S., Jiang, S. Y., & Li, Z. (2008). Petrogenesis of highly fractionated I-type granites in the coastal area of northeastern Fujian Province: Constraints from zircon U-Pb geochronology, geochemistry and Nd-Hf isotopes. *Acta Petroleii Sinica*, 24, 2468–2484. (in Chinese with English abstract).
- Rudnick, R., & Gao, S. (2003). Composition of the continental crust. In *Treatise on geochemistry* (Vol. 3) (pp. 1–64). Oxford: Elsevier.
- Salters, V. J. M., & Stracke, A. (2004). Composition of the depleted mantle. *Geochemistry, Geophysics, Geosystems*, 5, 1525–2027.
- Shan, Q., Zeng, Q. S., Li, J. K., Lu, H. Z., Hou, M. Z., Yu, X. Y., & Wu, C. J. (2014). U-Pb geochronology of zircon and geochemistry of Kuiqi miarolitic granites, Fujian Province. *Acta Petrologica Sinica*, 30, 1155–1167. (in Chinese with English abstract).
- Shao, F. L., Niu, Y. L., Regelous, R., & Zhu, D. C. (2015). Petrogenesis of peralkaline rhyolites in an intra-plate setting: Glass House Mountains, Southeast Queensland, Australia. *Lithos*, 216/217, 196–210.
- Shen, W. Z., Zhu, J. C., Liu, C. S., Xu, S. J., & Ling, H. F. (1993). Sm-Nd isotopic study of basement metamorphic rocks in South China and its constraint on material sources of granitoids. *Acta Petrologica Sinica*, 115–124, 9. (in Chinese with English abstract).
- Shu, L. S., Yu, J. H., & Wang, D. Z. (2000). Late Mesozoic granitic magmatism and metamorphism-ductile deformation in the Changle–Nanao Fault Zone, Fujian Province. *Geological Journal of China Universities*, 6, 368–378.
- Soderlund, U., Patchett, P. J., Vervoort, J. D., & Isachsen, C. E. (2004). The ^{176}Lu decay constant determined by Lu-Hf and U-Pb isotope systematics of Precambrian mafic intrusions. *Earth and Planetary Science Letters*, 219(3–4): 0–324.
- Song, S., Su, L., Li, X. H., Zhang, G., Niu, Y., & Zhang, L. (2010). Tracing the 850-Ma continental flood basalts from piece of subducted continental crust in the North Qaidam UHPM belt, NW China. *Precambrian Research*, 183, 805–816. <https://doi.org/10.1016/j.precamres.2010.09.008>
- Steiger, R. H., & E. Jäger. (1977). Subcommission on geochronology: Convention on the use of decay constants in geo- and cosmochronology. *Earth and Planetary Science Letters*, 36(3): 359–362.
- Sun, T. (2006). A new map showing the distribution of granites in South China and its explanatory notes. *Geological Bulletin of China*, 332–335, 25. (in Chinese with English abstract).
- Vervoort, J. D., & Blachert, J. (1999). Evolution of the depleted mantle: hafnium isotope evidence from juvenile rocks through time. *Geochimica et Cosmochimica Acta*, 63(3–4), 533–556.
- Wang, D. Z., & Shu, L. S. (2012). Late Mesozoic basin and range tectonics and related magmatism in Southeast China. *Geoscience Frontiers*, 3, 109–124. <https://doi.org/10.1016/j.gsf.2011.11.007>
- Wang, K. X., Sun, T., Chen, P. R., Ling, H. F., & Xiang, T. F. (2013). The geochronological and geochemical constraints on the petrogenesis of the Early Mesozoic A-type granite and diabase in northwestern Fujian province. *Lithos*, 179, 364–381. <https://doi.org/10.1016/j.lithos.2013.07.016>
- Whalen, J. B., Currie, K. L., & Chappell, B. W. (1987). A-type granites: Geochemical characteristics, discrimination and petrogenesis. *Contributions to Mineralogy and Petrology*, 95, 407–419. <https://doi.org/10.1007/BF00422022>
- Wiedenbeck, M. A. P. C., Alle, P., Corfu, F., Griffin, W. L., Meier, M., Oberli, F. V., ... Spiegel, W. (1995). Three natural zircon standards for U-Th-Pb, Lu-Hf, trace element and REE analyses. *Geostandards and Geoanalytical Research*, 19, 1–23. <https://doi.org/10.1111/j.1751-908X.1995.tb00147.x>
- Wu, C. L., Dong, S. W., Wu, D., Zhang, X., & Ernst, W. G. (2017). Late Mesozoic high-K calc-alkaline magmatism in Southeast China: The Tongling example. *International Geology Review*, 1–35.
- Wu, F. Y., Jahn, B. M., Wilde, S. A., Lo, C. H., Yui, T. F., Lin, Q., ... Sun, D. Y. (2003). Highly fractionated I-type granites in NE China (II): Isotopic geochemistry and implications for crustal growth in the Phanerozoic. *Lithos*, 67, 191–204. [https://doi.org/10.1016/S0024-4937\(03\)00015-X](https://doi.org/10.1016/S0024-4937(03)00015-X)
- Wu, F. Y., Li, X. H., Yang, J. H., & Zheng, Y. F. (2007). Discussions on the petrogenesis of granites. *Acta Petrologica Sinica*, 23, 1217–1238. (in Chinese with English abstract).
- Xiao, E., Qiu, J. S., Xu, X. S., Jiang, S. Y., Hu, J., & Li, Z. (2007). Geochronology and geochemistry of the Yaokeng alkaline granitic pluton in Zhejiang province: Petrogenetic and tectonic implications. *Acta Petrologica Sinica*, 23, 1431–1440.
- Yang, J. B., Zhao, Z. D., Hou, Q. Y., Niu, Y. L., Mo, X. X., Sheng, D., & Wang, L. L. (2018). Petrogenesis of Cretaceous (133–84 Ma) intermediate dykes and host granites in southeastern China: Implications for lithospheric extension, continental crustal growth, and geodynamics of paleo-Pacific subduction. *Lithos*, 296–299, 195–211. <https://doi.org/10.1016/j.lithos.2017.10.022>
- Zhou, X., & Yu, J. H. (2001). Geochemistry of the granitoids in Mesozoic metamorphic belt of coastal Fujian Province. *Geochimica*.
- Zhao, J. H., Hu, R. Z., Zhou, M. F., & Liu, S. (2007). Elemental and Sr-Nd-Pb isotopic geochemistry of Mesozoic mafic intrusions in southern Fujian Province, SE China: Implications for lithospheric mantle evolution. *Geological Magazine*, 144, 937–952.
- Zhao, J. L., Qiu, J. S., Liu, L., & Wang, R. Q. (2015). Geochronological, geochemical and Nd-Hf isotopic constraints on the petrogenesis of Late Cretaceous A-type granites from the southeastern coast of Fujian Province, South China. *Journal of Asian Earth Sciences*, 105, 338–359. <https://doi.org/10.1016/j.jseas.2015.01.022>
- Zhao, J. L., Qiu, J. S., Liu, L., & Wang, R. Q. (2016). The Late Cretaceous I- and A-type granite association of southeast China: Implications for the origin and evolution of post-collisional extensional magmatism. *Lithos*, 240, 16–33.
- Zhou, X. M., & Li, W. X. (2000). Origin of Late Mesozoic igneous rocks of southeastern China: Implications for lithosphere subduction and underplating of mafic magma. *Tectonophysics*, 326, 269–287. [https://doi.org/10.1016/S0040-1951\(00\)00120-7](https://doi.org/10.1016/S0040-1951(00)00120-7)
- Zhou, X. M., Sun, T., Shen, W. Z., Shu, L. S., & Niu, Y. L. (2006). Petrogenesis of Mesozoic granitoids and volcanic rocks in South China: A response to tectonic evolution. *Episodes*, 29, 26–33.

How to cite this article: Xue Q, Niu Y, Chen S, et al. Tectonic significance of the Cretaceous granitoids along the south-east coast of continental China. *Geological Journal*. 2020;55: 173–196. <https://doi.org/10.1002/gj.3388>

TABLE A1 Zircon U-Pb dating of the granitoids along the south-east coast of continental China

Analytical point	232Th ppm	238U ppm	Th/U Ratio	207Pb/206Pb		207Pb/235U		206Pb/238U		207Pb/206Pb		207Pb/235U		206Pb/238U		208Pb/232Th	
				Ratio	1sigma	Ratio	1sigma	Ratio	1sigma	Age (Ma)	1sigma	Age (Ma)	1sigma	Age (Ma)	1sigma	Age (Ma)	1sigma
FJS14-01																	
1	420	998	0.42	0.049	0.0016	0.106	0.0039	0.016	0.0004	153.8	75.9	102.2	3.6	101.3	2.5	101.5	2.8
2	140	698	0.20	0.051	0.0023	0.119	0.0068	0.017	0.0006	261.2	103.7	114.0	6.2	109.2	4.1	108.3	4.3
3	246	957	0.26	0.050	0.0014	0.113	0.0039	0.017	0.0004	183.4	69.4	109.0	3.5	105.9	2.6	110.6	4.1
4	268	875	0.31	0.048	0.0015	0.109	0.0040	0.017	0.0004	100.1	74.1	105.4	3.7	106.2	2.5	102.1	2.9
5	76	76	1.01	0.056	0.0063	0.100	0.0083	0.015	0.0005	455.6	250.0	96.6	7.7	97.8	3.3	96.7	5.2
6	312	1282	0.24	0.047	0.0014	0.097	0.0032	0.015	0.0003	33.4	61.1	94.3	3.0	96.8	2.1	96.5	2.7
7	87	134	0.65	0.049	0.0031	0.102	0.0060	0.016	0.0004	127.9	205.5	98.9	5.5	100.3	2.3	104.9	4.5
8	512	2664	0.19	0.048	0.0009	0.111	0.0027	0.017	0.0003	101.9	46.3	107.1	2.5	106.2	1.6	100.7	2.2
9	310	852	0.36	0.048	0.0015	0.105	0.0037	0.016	0.0003	122.3	70.4	101.5	3.4	100.4	2.1	99.8	2.7
10	89	171	0.52	0.047	0.0028	0.096	0.0052	0.015	0.0004	77.9	133.3	93.0	4.9	97.2	2.3	101.3	3.9
11	173	552	0.31	0.050	0.0015	0.105	0.0036	0.015	0.0003	198.2	104.6	101.0	3.3	97.0	1.8	100.6	3.1
FJS14-08																	
1	2484	4397	0.56	0.049	0.0010	0.122	0.0029	0.018	0.0004	127.9	46.3	117.3	2.6	116.4	2.3	118.6	2.3
2	3680	5033	0.73	0.048	0.0009	0.122	0.0029	0.018	0.0003	116.8	41.7	116.4	2.7	116.0	2.2	114.7	2.1
3	2975	4743	0.63	0.050	0.0008	0.131	0.0026	0.019	0.0003	211.2	38.9	125.2	2.4	120.4	1.8	121.8	2.1
4	2076	3336	0.62	0.050	0.0009	0.130	0.0027	0.019	0.0003	211.2	40.7	123.9	2.4	119.0	1.9	121.8	2.1
5	4200	7782	0.54	0.049	0.0008	0.125	0.0023	0.018	0.0003	200.1	35.2	119.4	2.1	117.3	1.7	121.6	1.9
6	3492	4447	0.79	0.050	0.0009	0.125	0.0028	0.018	0.0003	183.4	45.4	119.7	2.5	115.5	2.0	118.1	2.1
FJS14-13																	
1	640	300	2.13	0.049	0.0021	0.113	0.0046	0.017	0.0003	164.9	98.1	108.8	4.2	107.5	2.1	110.2	2.4
2	1203	458	2.63	0.050	0.0016	0.114	0.0039	0.017	0.0003	176.0	77.8	109.7	3.5	107.3	1.8	111.7	2.0
3	750	359	2.09	0.047	0.0017	0.111	0.0040	0.017	0.0003	57.5	85.2	106.7	3.7	109.0	1.8	109.7	2.1
4	623	652	0.95	0.048	0.0014	0.111	0.0034	0.017	0.0003	87.1	75.0	107.3	3.1	108.7	1.8	110.0	2.3
5	711	1023	0.69	0.047	0.0012	0.109	0.0029	0.017	0.0003	61.2	63.0	105.1	2.7	107.5	1.7	115.2	2.7
6	1275	845	1.51	0.047	0.0013	0.112	0.0033	0.017	0.0003	61.2	63.0	107.6	3.0	109.1	1.9	108.7	2.3
7	1565	829	1.89	0.049	0.0014	0.121	0.0038	0.018	0.0004	150.1	68.5	115.8	3.4	114.2	2.3	115.8	3.0
8	512	708	0.72	0.050	0.0016	0.118	0.0038	0.017	0.0003	198.2	75.9	112.8	3.4	109.0	2.0	111.6	3.0
9	387	488	0.79	0.049	0.0015	0.121	0.0039	0.018	0.0003	168.6	70.4	115.6	3.6	112.4	2.0	115.9	3.0
10	1269	1398	0.91	0.047	0.0010	0.111	0.0027	0.017	0.0003	55.7	42.6	107.2	2.5	109.0	1.8	107.8	2.2
11	733	1028	0.71	0.049	0.0012	0.115	0.0033	0.017	0.0003	164.9	57.4	110.3	3.0	107.0	2.0	110.6	2.4

TABLE A2 Geochronological data for the granitoids along the south-east coast of continental China

Sample	Locality	GPS	Rock type	Age (Ma)	Method	Reference
FJS14-01	Zhaohan	23°41'3.8"N, 117°3'16.9"E	Biotite granite	101 ± 3	LA-ICP-MS zircon U-Pb	This study
FJS14-02	Huxi	24°9'47.7"N, 117°48'23.4"E	Biotite monzogranite	96 ± 1	LA-ICP-MS zircon U-Pb	Qiu et al. (2012)
FJS14-03	Changqiao	24°14'39.3"N, 117°41'44.3"E	Biotite granite	119 ± 3	LA-ICP-MS zircon U-Pb	Qiu et al. (2012)
FJS14-04	Chengxi	24°25'12"N, 117°38'12.4"E	Alkali feldspar granite	101 ± 3	LA-ICP-MS zircon U-Pb	Qiu et al. (2012)
FJS14-05	Gunong	24°44'22.7"N, 117°43'2.4"E	Biotite monzogranite	97 ± 1	LA-ICP-MS zircon U-Pb	Chen et al. (2013)
FJS14-06	Changtai	24°34'57.8"N, 117°45'46.1"E	Granodiorite	100 ± 2; 103 ± 1	LA-ICP-MS zircon U-Pb	Chen et al. (2013)
FJS14-08	Xiamen	24°31'0.8"N, 118°2'22.3"E	Biotite granite	118 ± 2	LA-ICP-MS zircon U-Pb	This study
FJS14-09	Huacuo	24°39'32.7"N, 118°2'2.9"E	Biotite granite	111 ± 1	LA-ICP-MS zircon U-Pb	Li et al. (2012)
FJS14-11	Weitou	24°41'13.1"N, 118°22'15.8"E	Biotite monzogranite	100 ± 3	LA-ICP-MS zircon U-Pb	Liu et al. (2012)
FJS14-12	Quanzhou	24°54'11.3"N, 118°38'7.6"E	Monzogranite	108 ± 1	LA-ICP-MS zircon U-Pb	Li et al. (2012)
FJS14-13	Putian	25°24'31.3"N, 118°56'33.8"E	Monzogranite	109 ± 1	LA-ICP-MS zircon U-Pb	This study
FJS14-15	Kuiqi	26°00'47.8"N, 119°26'5.5"E	Alkali feldspar granite	95 ± 3	LA-ICP-MS zircon U-Pb	Lin et al. (2011)
FJS14-17	Danyang	26°21'33.9"N, 119°27'28.2"E	Granodiorite	100 ± 5	LA-ICP-MS zircon U-Pb	Lin et al. (2011)
FJS14-18	Sansha	26°55'45.2"N, 120°09'51.7"E	Alkali feldspar granite	92 ± 2	LA-ICP-MS zircon U-Pb	Qiu et al. (2008)
FJS14-20	Dacengshan	27°0'21.8"N, 120°13'54.7"E	Graphic granite	93 ± 2	LA-ICP-MS zircon U-Pb	Qiu et al. (2008)
FJS14-22	Nanzhen	27°7'9.8"N, 120°22'19.5"E	Graphic granite	96 ± 3	LA-ICP-MS zircon U-Pb	Qiu et al. (2008)

TABLE A3 Whole-rock major elements compositions of the granitoids along the south-east coast of continental China

Rock type Sample	Biotite monzogranite FJS14-05	Biotite monzogranite FJS14-06host	Granodiorite FJS14-06MME	Biotite monzogranite FJS14-17host	Granodiorite FJS14-17MME	Biotite granite FJS14-01	Biotite monzogranite FJS14-02	Biotite granite FJS14-03	Biotite granite FJS14-08
SiO ₂	68.41	62.16	60.66	64.72	56.95	71.85	75.02	73.35	75.94
TiO ₂	0.48	0.58	0.71	0.61	1.03	0.21	0.22	0.17	0.07
Al ₂ O ₃	14.68	17.64	18.25	15.92	16.62	14.22	12.45	13.67	12.98
TFe ₂ O ₃	3.06	4.56	6.14	3.59	7.15	1.94	1.21	1.29	0.47
MnO	0.09	0.08	0.11	0.09	0.18	0.06	0.04	0.09	0.04
MgO	0.89	1.43	2.05	1.43	3.27	0.43	0.27	0.34	0.07
CaO	2.27	4.75	4.85	3.10	5.61	2.27	0.90	1.31	0.49
Na ₂ O	3.86	4.19	3.16	3.88	5.50	3.72	3.48	3.91	4.01
K ₂ O	4.65	3.36	4.67	5.24	1.60	3.89	5.11	4.77	4.91
P ₂ O ₅	0.14	0.23	0.30	0.15	0.36	0.07	0.04	0.04	0.00
LOI	0.78	0.40	0.89	0.61	1.16	0.60	0.50	0.32	0.24
Total	99.31	99.37	101.80	99.35	99.42	99.27	99.24	99.26	99.23
A/NK	1.29	1.67	1.78	1.32	1.54	1.37	1.10	1.18	1.09
A/CNK	0.95	0.92	0.96	0.90	0.79	0.98	0.96	0.98	1.01

Note. A/NK = molar Al₂O₃/(Na₂O + K₂O); A/CNK = molar Al₂O₃/(CaO + Na₂O + K₂O); LOI: loss on ignition.

TABLE A3 Whole-rock major elements compositions of the granitoids along the south-east coast of continental China

Rock type Sample	Biotite granite FJS14-09	Biotite monzogranite FJS14-11	Monzogranite FJS14-12	Monzogranite FJS14-13	Graphic granite FJS14-20	Graphic granite FJS14-22	Alkali feldspar granite FJS14-04	Alkali feldspar granite FJS14-15	Alkali feldspar granite FJS14-18
SiO ₂	68.80	74.56	75.28	75.70	72.51	75.42	75.25	75.93	76.32
TiO ₂	0.23	0.16	0.10	0.13	0.26	0.13	0.08	0.13	0.11
Al ₂ O ₃	16.07	13.44	12.74	12.36	13.76	12.42	13.13	11.71	12.26
TFe ₂ O ₃	1.48	0.84	0.68	0.85	1.55	1.05	0.63	1.31	0.78
MnO	0.05	0.03	0.04	0.03	0.06	0.09	0.08	0.12	0.09
MgO	0.30	0.20	0.28	0.17	0.31	0.19	0.04	0.05	0.06
CaO	1.39	0.79	1.23	0.84	0.76	0.66	0.43	0.25	0.33
Na ₂ O	4.99	4.25	3.95	4.11	4.53	4.36	4.45	4.71	4.59
K ₂ O	5.58	4.68	4.78	4.61	4.74	4.48	4.82	4.58	4.49
P ₂ O ₅	0.04	0.02	0.01	0.01	0.07	0.03	0.00	(0.00)	0.00
LOI	0.37	0.27	0.15	0.40	0.70	0.42	0.34	0.45	0.21
Total	99.31	99.25	99.24	99.24	99.27	99.24	99.24	99.23	99.23
A/NK	1.13	1.11	1.09	1.05	1.09	1.03	1.05	0.92	0.99
A/CNK	0.96	0.99	0.91	0.93	0.98	0.94	0.99	0.89	0.94

TABLE A4 Whole-rock trace elements compositions of the granitoids along the south-east coast of continental China

Rock type Sample	Blank	W-2	GSP-2	BHVO-2	AGV-2	BCR-2	Biotite monzogranite FJS14-05	Biotite monzogranite FJS14-06host	Granodiorite FJS14-06MME	Biotite monzogranite FJS14-17host	Granodiorite FJS14-17MME	Biotite granite FJS14-01
Rb	0.011	20	244	240	9	68	48	148	121	184	241	135
Ba	0.036	171	1412	1397	135	1192	718	1005	810	1503	765	780
Th	0.00	2.1	111	114	1.2	6.1	5.9	30	17	19	20	14
U	0.00	0.52	2.5	2.7	0.43	2.0	1.8	5.5	4.4	5.2	5.5	4.0
Ta	0.00	0.46	0.86	0.85	1.2	0.84	0.77	1.1	0.73	0.66	1.4	1.3
Nb	0.00	7.1	26	25	18	14	12	16	10	12	17	14
Pb	0.037	7.5	40	41	1.5	13	9.9	31	19	18	24	26
Sr	0.11	208	249	242	431	700	360	348	637	635	279	420
Zr	0.025	94	492	490	174	231	185	159	109	59	123	65
Hf	0.0000	2.6	13	13	4.6	5.4	5.1	4.2	3.1	2.0	3.8	3.4
Y	0.0009	21	26	26	26	19	35	26	14	15	30	27
La	0.0020	11	190	191	16	39	26	63	39	24	32	52
Ce	0.0010	23	451	453	39	71	55	119	76	54	74	70
Pr	0.0000	3.0	57	57	5.5	8.3	6.9	13	8.6	6.4	8.9	11
Nd	0.0005	13	214	217	25	31	29	42	30	23	32	40
Sm	0.0000	3.3	26	26	6.2	5.5	6.7	7.2	5.2	4.5	6.3	8.3
Eu	0.0000	1.1	2.3	2.2	2.1	1.5	2.0	1.5	1.2	1.1	1.0	2.3
Gd	0.0000	3.9	13	13	6.5	4.6	7.0	6.0	4.2	3.9	5.5	7.3
Tb	0.0000	0.62	1.3	1.3	0.96	0.65	1.1	0.86	0.55	0.53	0.89	1.1
Dy	0.0003	3.8	5.7	5.8	5.4	3.5	6.4	4.7	2.7	2.7	5.0	5.8
Ho	0.0000	0.79	0.95	0.96	1.0	0.68	1.3	0.98	0.53	0.55	1.1	1.0
Er	0.0000	2.3	2.4	2.4	2.7	1.9	3.8	2.7	1.3	1.4	3.0	2.5
Tm	0.0000	0.32	0.29	0.30	0.35	0.27	0.55	0.42	0.20	0.22	0.49	0.38
Yb	0.0001	2.0	1.7	1.6	2.0	1.6	3.4	2.8	1.2	1.4	3.2	2.4
Lu	0.0000	0.31	0.23	0.24	0.28	0.26	0.52	0.42	0.18	0.21	0.46	0.33
Ga	0.0000	18	24	23	23	21	23	17	21	20	15	19
10,000 × Ga/Al							2.13	2.29	2.04	1.82	2.43	2.47
ΣREE							265	172	125	173	301	204
(La/Yb) _N							16.33	22.71	12.20	7.39	8.39	15.72
(La/Sm) _N							5.67	4.83	3.40	3.31	3.66	4.06
(Gd/Yb) _N							1.78	2.80	2.29	1.45	1.46	2.55
Eu/Eu [*]							0.67	0.76	0.76	0.49	0.39	0.87
Rb/Sr							0.43	0.19	0.29	0.86	0.35	0.32

Note. (La/Yb)_N is chondrite-normalized La/Yb; (La/Sm)_N is chondrite-normalized La/Sm; (Gd/Yb)_N is chondrite-normalized Gd/Yb; Eu/Eu^{*} = Eu_N × 2/(Sm_N + Gd_N), where subscript N refers to chondrite-normalized value.

TABLE A4 Whole-rock trace elements compositions of the granitoids along the south-east coast of continental China

Rock type Sample	Biotite monzogranite FJS14-02	Biotite granite FJS14-03	Biotite granite FJS14-08	Biotite granite FJS14-11	Biotite monzogranite FJS14-09	Monzogranite FJS14-12	Monzogranite FJS14-13	Graphic granite FJS14-20	Graphic granite FJS14-22	Graphic granite FJS14-20	Alkali feldspar granite FJS14-04	Alkali feldspar granite FJS14-15	Alkali feldspar granite FJS14-18
Rb	253	153	181	171	127	215	217	179	219	386	228	186	
Ba	536	546	174	524	805	257	729	684	290	8	6	12	
Th	40	21	16	41	12	36	34	18	25	32	16	18	
U	8.3	6.9	7.5	5.9	3.3	12.1	4.3	3.1	5.9	8.3	5.6	2.8	
Ta	2.2	1.8	1.6	2.2	1.1	1.2	1.2	1.0	1.4	2.5	2.3	1.2	
Nb	21	21	16	23	12	14	17	18	19	31	39	20	
Pb	37	21	23	14	26	31	26	24	29	39	21	26	
Sr	128	178	33	121	129	97	117	140	70	10	2	7	
Zr	151	73	60	128	67	82	92	176	101	72	262	112	
Hf	5.0	2.6	2.6	4.9	2.8	3.3	3.3	5.6	4.4	4.7	8.7	4.7	
Y	25	27	24	23	20	16	17	24	28	56	52	20	
La	58	24	20	42	27	27	38	52	35	36	25	25	
Ce	107	47	45	80	56	50	73	95	66	40	54	49	
Pr	11	5.3	5.1	8.2	6.4	5.0	7.5	9.7	6.7	9.6	5.9	4.8	
Nd	34	18	17	25	22	15	23	31	21	31	19	13	
Sm	5.7	3.9	3.8	4.1	4.1	2.4	4.1	5.3	3.6	8.0	5.0	2.5	
Eu	0.65	0.59	0.39	0.54	0.62	0.31	0.56	0.80	0.35	0.16	0.32	0.12	
Gd	4.8	3.7	3.4	3.6	3.6	2.1	3.3	4.3	3.3	7.0	5.7	2.3	
Tb	0.76	0.66	0.60	0.54	0.57	0.34	0.51	0.68	0.56	1.2	1.1	0.42	
Dy	4.4	4.2	3.7	3.2	3.3	2.0	2.7	4.0	3.7	7.1	7.1	2.6	
Ho	0.94	0.93	0.81	0.75	0.71	0.49	0.57	0.82	0.83	1.5	1.7	0.63	
Er	2.8	2.7	2.3	2.4	2.0	1.6	1.6	2.5	2.8	4.5	5.3	2.0	
Tm	0.46	0.45	0.40	0.46	0.34	0.29	0.27	0.38	0.49	0.72	0.91	0.36	
Yb	3.1	3.1	2.6	3.4	2.2	2.1	1.8	2.6	3.4	4.9	6.3	2.5	
Lu	0.48	0.48	0.41	0.58	0.35	0.38	0.29	0.43	0.56	0.74	0.99	0.41	
Ga	16	15	13	14	14	13	13	18	16	20	21	16	
10,000 × Ga/Al	2.40	2.04	1.89	1.64	1.95	1.92	2.03	2.41	2.49	2.84	3.45	2.43	
ΣREE	234	115	105	175	129	109	157	209	149	152	139	106	
(La/Yb) _N	13.11	5.49	5.60	8.99	8.83	8.99	15.05	14.18	7.31	5.32	2.84	7.10	
(La/Sm) _N	6.46	3.97	3.43	6.55	4.25	7.33	6.02	6.37	6.26	2.91	3.23	6.61	
(Gd/Yb) _N	1.27	0.97	1.10	0.88	1.36	0.81	1.51	1.36	0.78	1.19	0.75	0.76	
Eu/Eu [*]	0.37	0.47	0.32	0.42	0.48	0.42	0.45	0.50	0.31	0.06	0.19	0.16	
Rb/Sr	1.99	0.86	5.42	1.41	0.99	2.21	1.86	1.28	3.15	36.90	103.51	24.84	

TABLE A5 Microprobe analysis of representative plagioclase of the granitoids along the south-east coast of continental China

Analytical point	SiO ₂	TiO ₂	Al ₂ O ₃	FeO	MnO	MgO	CaO	Na ₂ O	K ₂ O	Total	Si	Al	Ca	Na	K	O	Si(8)	Al(8)	Ca(8)	Na(8)	K(8)	An	Ab	Or	
FJS14-06host																									
1	59.59	0.00	25.34	0.19	0.00	0.02	6.78	7.26	0.37	99.55	0.99	0.50	0.12	0.23	0.01	2.97	2.67	1.34	0.33	0.63	0.02	33	65	2	
2	58.48	0.01	26.11	0.29	0.00	0.06	7.93	6.54	0.51	99.93	0.97	0.51	0.14	0.21	0.14	3.03	2.57	1.35	0.37	0.56	0.37	29	43	28	
3	57.38	0.04	26.74	0.29	0.01	0.00	8.46	6.41	0.25	99.59	0.96	0.52	0.15	0.21	0.14	3.02	2.53	1.39	0.40	0.55	0.36	31	42	28	
4	57.08	0.02	26.99	0.24	0.02	0.00	8.70	6.22	0.19	99.45	0.95	0.53	0.16	0.20	0.13	3.02	2.52	1.40	0.41	0.53	0.35	32	41	27	
5	58.65	0.00	25.92	0.20	0.02	0.01	7.50	6.78	0.36	99.43	0.98	0.51	0.13	0.22	0.14	3.03	2.58	1.34	0.35	0.58	0.38	27	44	29	
6	58.09	0.00	26.48	0.24	0.00	0.00	8.00	6.63	0.33	99.76	0.97	0.52	0.14	0.21	0.14	3.04	2.55	1.37	0.38	0.56	0.37	29	43	28	
7	59.25	0.00	25.87	0.22	0.00	0.02	7.54	6.73	0.45	100.09	0.99	0.51	0.13	0.22	0.14	3.05	2.59	1.33	0.35	0.57	0.38	27	44	29	
8	58.49	0.00	25.89	0.24	0.01	0.00	7.55	6.83	0.35	99.35	0.97	0.51	0.13	0.22	0.15	3.03	2.57	1.34	0.36	0.58	0.38	27	44	29	
9	55.19	0.00	28.14	0.21	0.01	0.00	9.95	5.25	0.19	98.93	0.92	0.55	0.18	0.17	0.11	2.99	2.46	1.48	0.48	0.45	0.30	39	37	24	
10	57.56	0.03	26.25	0.21	0.00	0.02	8.57	6.41	0.27	99.32	0.96	0.51	0.15	0.21	0.14	3.02	2.55	1.37	0.41	0.55	0.36	31	42	27	
11	57.65	0.00	26.39	0.23	0.01	0.01	8.23	6.48	0.37	99.37	0.96	0.52	0.15	0.21	0.14	3.02	2.55	1.37	0.39	0.55	0.37	30	42	28	
12	59.11	0.00	25.46	0.26	0.00	0.00	7.03	7.10	0.38	99.35	0.99	0.50	0.13	0.23	0.15	3.03	2.60	1.32	0.33	0.60	0.40	25	45	30	
13	58.56	0.00	25.77	0.28	0.00	0.00	7.36	6.71	0.30	98.97	0.98	0.51	0.13	0.22	0.14	3.02	2.58	1.34	0.35	0.57	0.38	27	44	29	
14	56.08	0.00	27.48	0.26	0.00	0.00	9.16	5.91	0.21	99.11	0.93	0.54	0.16	0.19	0.13	3.00	2.49	1.44	0.44	0.51	0.34	34	40	26	
15	59.39	0.00	25.54	0.25	0.00	0.00	7.12	7.08	0.27	99.66	0.99	0.50	0.13	0.23	0.15	3.05	2.60	1.31	0.33	0.60	0.40	25	45	30	
16	58.48	0.00	26.34	0.25	0.03	0.02	7.85	6.63	0.23	99.83	0.97	0.52	0.14	0.21	0.14	3.04	2.56	1.36	0.37	0.56	0.37	28	43	28	
17	57.99	0.03	26.66	0.23	0.00	0.01	8.34	6.61	0.26	100.12	0.97	0.52	0.15	0.21	0.14	3.04	2.54	1.37	0.39	0.56	0.37	30	42	28	
18	57.75	0.02	26.51	0.25	0.00	0.00	8.15	6.58	0.24	99.50	0.96	0.52	0.15	0.21	0.14	3.03	2.54	1.37	0.38	0.56	0.37	29	43	28	
19	57.47	0.03	26.68	0.25	0.00	0.00	8.36	6.45	0.22	99.46	0.96	0.52	0.15	0.21	0.14	3.02	2.54	1.38	0.40	0.55	0.36	30	42	28	
20	59.01	0.01	25.90	0.22	0.00	0.02	7.62	6.93	0.23	99.93	0.98	0.51	0.14	0.22	0.15	3.05	2.58	1.33	0.36	0.59	0.39	27	44	29	
FJS14-06MME																									
1	55.75	0.00	27.75	0.24	0.04	0.03	9.26	5.69	0.17	98.93	0.93	0.54	0.17	0.18	0.00	2.93	2.53	1.48	0.45	0.50	0.01	47	52	1	
2	55.87	0.04	28.02	0.22	0.02	0.00	9.58	5.73	0.17	99.65	0.93	0.55	0.17	0.18	0.00	2.95	2.52	1.49	0.46	0.50	0.01	48	51	1	
3	55.96	0.00	27.92	0.19	0.00	0.00	9.47	5.85	0.22	99.60	0.93	0.55	0.17	0.19	0.00	2.95	2.53	1.48	0.46	0.51	0.01	47	52	1	
4	56.50	0.00	27.17	0.22	0.01	0.00	9.07	6.01	0.20	99.18	0.94	0.53	0.16	0.19	0.00	2.94	2.56	1.45	0.44	0.53	0.01	45	54	1	
5	56.22	0.03	26.06	0.20	0.01	0.01	8.14	6.22	0.20	97.09	0.94	0.51	0.15	0.20	0.00	2.89	2.60	1.42	0.40	0.56	0.01	41	57	1	
6	57.65	0.00	26.61	0.23	0.01	0.00	8.10	6.63	0.20	99.44	0.96	0.52	0.14	0.21	0.00	2.96	2.60	1.41	0.39	0.58	0.01	40	59	1	
7	56.18	0.00	27.38	0.22	0.03	0.02	9.34	5.81	0.17	99.14	0.94	0.54	0.17	0.19	0.00	2.94	2.55	1.46	0.45	0.51	0.01	47	52	1	
8	57.20	0.00	26.99	0.26	0.03	0.00	8.64	6.24	0.18	99.54	0.95	0.53	0.15	0.20	0.00	2.96	2.58	1.43	0.42	0.54	0.01	43	56	1	
9	53.66	0.00	29.28	0.23	0.04	0.00	10.99	4.83	0.22	99.24	0.89	0.57	0.20	0.16	0.00	2.93	2.45	1.57	0.54	0.43	0.01	55	44	1	
10	56.27	0.00	27.24	0.23	0.00	0.02	8.84	6.09	0.17	98.86	0.94	0.53	0.16	0.20	0.00	2.93	2.56	1.46	0.43	0.54	0.01	44	55	1	

(Continues)

TABLE A5 (Continued)

	Analytical point	SiO ₂	TiO ₂	Al ₂ O ₃	FeO	MnO	MgO	CaO	Na ₂ O	K ₂ O	Total	Si	Al	Ca	Na	K	O	Si(8)	Al(8)	Ca(8)	Na(8)	K(8)	An	Ab	Or
FJS14-17host																									
1	57.21	0.05	26.14	0.30	0.00	0.00	8.07	6.33	0.30	98.41	0.95	0.51	0.14	0.20	0.01	2.93	2.61	1.40	0.39	0.56	0.02	41	58	2	
2	57.34	0.00	26.08	0.36	0.00	0.02	7.96	6.49	0.36	98.61	0.96	0.51	0.14	0.21	0.01	2.93	2.61	1.40	0.39	0.57	0.02	40	58	2	
3	61.01	0.00	23.89	0.25	0.03	0.00	5.09	8.16	0.42	98.85	1.02	0.47	0.09	0.26	0.01	2.96	2.75	1.26	0.25	0.71	0.02	25	72	2	
4	57.40	0.04	25.84	0.36	0.01	0.02	7.95	6.56	0.40	98.57	0.96	0.51	0.14	0.21	0.01	2.93	2.62	1.39	0.39	0.58	0.02	39	58	2	
5	60.52	0.00	23.97	0.24	0.04	0.00	5.45	8.00	0.24	98.45	1.01	0.47	0.10	0.26	0.01	2.95	2.73	1.27	0.26	0.70	0.01	27	72	1	
6	62.03	0.01	23.08	0.20	0.00	0.00	4.71	8.50	0.65	99.18	1.03	0.45	0.08	0.27	0.01	2.97	2.78	1.22	0.23	0.74	0.04	23	74	4	
7	57.59	0.00	26.12	0.34	0.00	0.01	7.97	6.58	0.30	98.91	0.96	0.51	0.14	0.21	0.01	2.94	2.61	1.39	0.39	0.58	0.02	39	59	2	
8	58.02	0.06	25.71	0.20	0.01	0.01	7.23	7.17	0.25	98.65	0.97	0.50	0.13	0.23	0.01	2.94	2.63	1.37	0.35	0.63	0.01	35	63	1	
9	57.97	0.01	25.56	0.36	0.00	0.03	7.33	6.95	0.29	98.50	0.97	0.50	0.13	0.22	0.01	2.93	2.64	1.37	0.36	0.61	0.02	36	62	2	
10	57.40	0.07	25.82	0.36	0.03	0.01	7.68	6.64	0.50	98.52	0.96	0.51	0.14	0.21	0.01	2.92	2.62	1.39	0.38	0.59	0.03	38	59	3	
FJS14-17MME																									
1	55.15	0.02	27.72	0.35	0.00	0.01	9.24	5.55	0.36	98.39	0.92	0.54	0.16	0.18	0.01	2.91	2.53	1.49	0.45	0.49	0.02	47	51	2	
2	55.68	0.00	27.45	0.31	0.01	0.00	9.29	5.64	0.39	98.77	0.93	0.54	0.17	0.18	0.01	2.92	2.54	1.47	0.45	0.50	0.02	47	51	2	
3	56.91	0.06	26.51	0.31	0.00	0.01	8.15	6.23	0.44	98.62	0.95	0.52	0.15	0.20	0.01	2.93	2.59	1.42	0.40	0.55	0.03	41	56	3	
4	56.55	0.02	26.58	0.29	0.03	0.03	8.37	6.16	0.33	98.35	0.94	0.52	0.15	0.20	0.01	2.92	2.58	1.43	0.41	0.54	0.02	42	56	2	
5	58.87	0.04	24.97	0.37	0.00	0.00	6.65	7.06	0.53	98.49	0.98	0.49	0.12	0.23	0.01	2.94	2.67	1.33	0.32	0.62	0.03	33	64	3	
6	59.21	0.03	25.04	0.31	0.00	0.02	6.48	7.16	0.42	98.66	0.99	0.49	0.12	0.23	0.01	2.95	2.68	1.33	0.31	0.63	0.02	33	65	3	
7	55.88	0.05	26.98	0.31	0.00	0.01	8.94	5.87	0.27	98.31	0.93	0.53	0.16	0.19	0.01	2.91	2.56	1.45	0.44	0.52	0.02	45	53	2	
8	55.46	0.03	26.87	0.26	0.03	0.03	8.85	5.85	0.37	97.74	0.92	0.53	0.16	0.19	0.01	2.90	2.55	1.46	0.44	0.52	0.02	45	53	2	
9	55.42	0.06	26.77	0.37	0.00	0.01	8.87	5.88	0.31	97.70	0.92	0.52	0.16	0.19	0.01	2.89	2.56	1.45	0.44	0.53	0.02	45	53	2	

Note. Structural formulas on the basis of eight oxygen atoms.

TABLE A6 Whole rock Sr–Nd–Hf isotopic composition for the granitoids along the south-east coast of continental China

Sample no.	(1/Sr) * 1,000			87Sr/86Sr			143Nd/144Nd			Nd			176Hf/177Hf								
	Rb (ppm)	Sr (ppm)	Ratio	±2σ	87Sr/86Sr _(l)	Sr (ppm)	Nd (ppm)	Ratio	±2σ	143Nd/ 144Nd _(l)	T _{DM} (Ga)	T _{DM} 2 (Ga)	Lu (ppm)	Hf (ppm)	176Hf/ 177Hf _(l)	Ratio	±2σ	176Hf/ 177Hf _(l)	Ratio	±2σ	Age (Ma)
FJS14-05	148	348	2.87	0.708418	0.000008	0.70669	7.20	42.4	0.512366	0.000007	0.51230	-4.14	1.08	0.418	4.24	0.282672	0.000005	0.28265	-2.31	97	
FJS14-06host	121	637	1.57	0.706757	0.000008	0.70596	5.22	30.1	0.512412	0.000005	0.51234	-3.24	1.03	1.18	0.180	3.13	0.282699	0.000004	0.28268	-0.92	100
FJS14-06MME	184	635	1.57	0.707180	0.000009	0.70593	4.54	23.2	0.512417	0.000007	0.51234	-3.29	—	—	0.210	2.05	0.282721	0.000005	0.28269	-0.55	103
FJS14-17host	241	279	3.58	0.711189	0.000008	0.70763	6.33	31.8	0.512276	0.000007	0.51220	-6.09	1.43	1.42	0.460	3.82	0.282610	0.000005	0.28258	-4.68	100
FJS14-17MME	127	359	2.78	0.709143	0.000010	—	10.2	54.4	0.512276	0.000006	—	—	—	—	0.777	2.82	0.282656	0.000004	—	—	—
FJS14-01	135	420	2.38	0.707295	0.000009	0.70594	8.28	39.6	0.512419	0.000007	0.51234	-3.37	1.28	1.20	0.332	3.38	0.282706	0.000005	0.28268	-1.05	101
FJS14-02	253	128	7.84	0.712909	0.000008	0.70498	5.75	33.9	0.512519	0.000006	0.51246	-1.16	0.86	1.01	0.479	4.97	0.282832	0.000005	0.28281	3.35	96
FJS14-03	153	178	5.61	0.709710	0.000009	0.70543	3.87	17.9	0.512496	0.000006	0.51240	-1.76	1.19	1.08	0.480	2.62	0.282787	0.000005	0.28273	1.12	119
FJS14-08	181	33	29.86	0.732072	0.000009	0.70521	3.78	16.7	0.512482	0.000006	0.51238	-2.13	1.32	1.11	0.410	2.64	0.282772	0.000005	0.28272	0.88	118
FJS14-09	171	121	8.24	0.712875	0.000008	0.70635	4.15	25.3	0.512415	0.000006	0.51234	-2.97	0.98	1.17	0.576	4.94	0.282741	0.000005	0.28271	0.13	111
FJS14-11	127	129	7.76	0.709920	0.000008	0.70577	4.12	21.8	0.512438	0.000006	0.51236	-2.86	1.09	1.15	0.348	2.76	0.282773	0.000004	0.28274	1.06	100
FJS14-12	215	97	10.30	0.715265	0.000009	0.70633	2.37	14.7	0.512438	0.000006	0.51237	-2.53	0.93	1.13	0.376	3.34	0.282767	0.000005	0.28273	1.05	108
FJS14-13	217	117	8.54	0.714844	0.000010	0.70644	4.09	23.2	0.512317	0.000007	0.51224	-5.02	1.18	1.34	0.290	3.26	0.282660	0.000005	0.28263	-2.48	109
FJS14-20	179	140	7.14	0.712614	0.000009	0.70773	5.27	31.2	0.512293	0.000007	0.51223	-5.61	1.17	1.37	0.427	5.63	0.282627	0.000004	0.28261	-3.76	93
FJS14-22	219	70	14.38	0.708390	0.000008	0.69594	3.62	21.0	0.512278	0.000006	0.51221	-5.89	1.21	1.40	0.560	4.40	0.282636	0.000004	0.28260	-3.84	96
FJS14-04	386	10	95.59	0.853680	0.000010	0.69696	7.98	31.1	0.512391	0.000006	0.51229	-4.29	1.98	1.27	0.743	4.72	0.282660	0.000004	0.28262	-3.23	101
FJS14-15	228	2	454.79	1.131078	0.000016	0.73611	5.00	19.2	0.512459	0.000007	0.51236	-3.02	1.87	1.16	0.990	8.74	0.282754	0.000004	0.28273	0.43	95
FJS14-18	186	7	133.82	0.805482	0.000012	0.70978	2.46	13.5	0.512288	0.000006	0.51222	-5.81	1.27	1.39	0.406	4.68	0.282631	0.000004	0.28261	-3.73	92

^a87Sr/86Sr_(l) = [(⁸⁷Rb/⁸⁶Sr)(e^{λt} - 1)], where λ(⁸⁷Rb) = 1.42 × 10⁻¹¹ year⁻¹ (Steriger & Jager, 1977), ^b143Nd/144Nd_(l) = [(¹⁴³Nd/¹⁴⁴Nd)(e^{λt} - 1)], ^cNd_(l) = [(¹⁴³Nd/¹⁴⁴Nd)(e^{λt} - 1)], where λ(¹⁴³Nd) = 6.54 × 10⁻¹² year⁻¹ (Lugmair & Marti, 1978), ^d147Sm/144Nd_{CHUR} = 0.512638, ^e147Sm/144Nd_{DM} = 0.2137, ^f147Sm/144Nd_{CHUR} = 0.51315, and ^g147Sm/144Nd_{DM} = 0.12, c¹⁷⁶Hf/¹⁷⁷Hf_(l) = [(¹⁷⁶Hf/¹⁷⁷Hf)(e^{λt} - 1)], ^hHf_(l) = [(¹⁷⁶Hf/¹⁷⁷Hf)(e^{λt} - 1)] × 10⁻¹¹ year⁻¹ (Soderlund et al., 2004), ⁱ¹⁷⁶Lu/¹⁷⁷Lu_{CHUR} = 1.867 × 10⁻¹¹ year⁻¹ (Vervoort & Blinchert-Toft, 1999), and ^j¹⁷⁶Lu/¹⁷⁷Hf_{DM} = 0.0384, ^k¹⁷⁶Lu/¹⁷⁷Hf_{CHUR} = 0.283251 (Vervoort & Blinchert-Toft, 1999), and ^l¹⁷⁶Lu/¹⁷⁷Hf_{CC} = 0.0105 (Griffin et al., 2002).

TABLE A7 Whole-rock major elements composition data from literature

Locality	Gunong a	Changtai 08JH310	Huxi b	Huxi b	Changqiao b	Xincun a	Huacuo c	Weitou d, e	Quanzhou c	Daceng shan	Daceng shan	Daceng shan	Daceng shan	Daceng shan	Daceng shan
Reference Sample	08JH332	08JH310	ZP-4	ZP-5	ZP-6	ZP-7	08JH312	08JH324	HC-4	DCS-1	DCS-2	DCS-1	DCS-2	DCS-1	DCS-2
SiO ₂	69.12	63.45	70.14	69.67	76.10	76.07	76.50	77.58	72.82	70.25	75.94	70.56	75.67	76.06	77.17
TiO ₂	0.43	0.73	0.32	0.38	0.09	0.08	0.08	0.09	0.22	0.35	0.12	0.24	0.16	0.14	0.13
Al ₂ O ₃	14.86	16.35	15.00	14.77	13.05	12.94	12.98	12.56	13.78	14.23	12.91	15.42	12.92	12.63	12.75
TFe ₂ O ₃	2.87	5.39	2.54	3.34	0.89	0.78	0.62	0.65	1.71	3.79	0.69	1.86	1.02	1.03	0.85
MnO	0.08	0.08	0.09	0.09	0.09	0.09	0.08	0.07	0.05	0.15	0.05	0.05	0.08	0.07	0.06
MgO	0.86	2.07	0.79	0.97	0.06	0.04	0.06	0.09	0.48	1.20	0.18	0.52	0.20	0.21	0.22
CaO	2.22	4.69	2.20	2.92	0.74	0.69	0.48	0.54	1.76	3.64	0.87	2.32	0.43	0.39	0.51
Na ₂ O	3.93	3.38	4.07	3.49	3.81	3.79	4.25	3.97	3.95	3.52	3.42	3.90	4.45	4.33	4.18
K ₂ O	4.29	3.06	4.18	3.14	4.80	4.88	4.72	4.41	4.51	1.74	5.12	3.98	4.74	4.76	4.58
P ₂ O ₅	0.14	0.21	0.16	0.17	0.07	0.06	0.01	0.01	0.10	0.20	0.06	0.12	0.06	0.06	0.05
LOI	0.58	0.54	0.82	1.00	0.54	0.69	0.30	0.34	0.44	0.69	0.38	0.63	0.49	0.43	0.47
Total	99.38	99.95	100.31	99.94	100.24	100.11	100.08	100.31	99.82	99.76	99.74	99.60	100.22	100.11	100.05
A/NK	1.34	1.84	1.32	1.43	1.13	1.08	1.07	1.11	1.21	1.85	1.15	1.44	1.04	1.03	1.08
A/CNK	0.98	0.94	0.89	1.24	1.02	1.01	1.00	1.02	0.94	0.99	1.01	1.03	0.98	0.97	1.00
SiO ₂ /MgO	80.4	30.7	88.8	71.8	1268.3	1901.8	1275.0	862.0	151.7	58.5	421.9	135.7	378.4	362.2	346.5

Note. A/NK = molar Al₂O₃/(Na₂O + K₂O); A/CNK = molar Al₂O₃/(CaO + Na₂O + K₂O); LOI: loss on ignition.^aChen et al. (2013); b: Qiu et al. (2012); c: Li et al. (2012); d: Liu et al. (2012); e: Zhou and Yu (2001); f: Qiu et al. (2008).

TABLE A8 Whole-rock trace elements composition data from literature

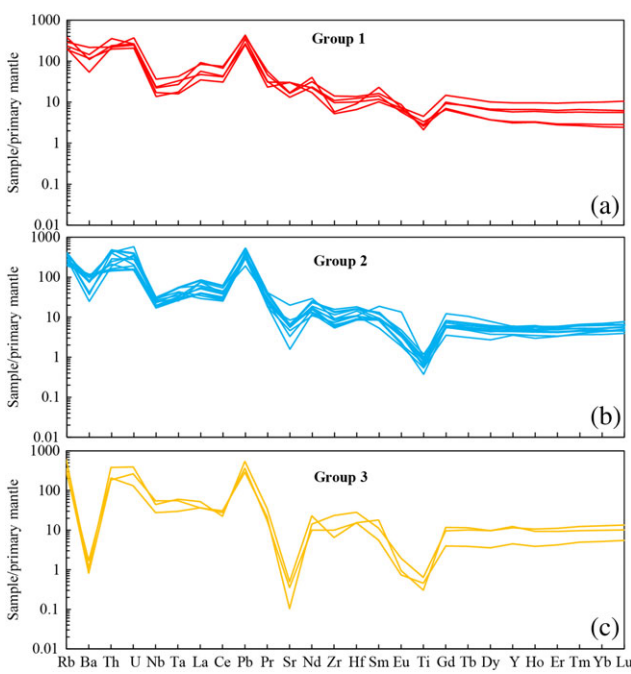
Locality	Gunong	Changtai	Huxi	Huxi	Changqiao	Xincun	Xincun	Huacao	Weitou	Quanzhou	Dacengshan	Nanzhen	Chengxi	Sansha	
Reference	a	b	b	b	b	a	a	c	d, e	f	f	f	b	f	
Sample	08JH332	08JH310	ZP-4	ZP-5	ZP-6	08JH312	08JH324	HC-4	WT-1	QZ-7	DCS-1	DCS-2	ZP-8	SAN-2	
Rb	178	158	116	129	200	210	268	104	63	172	93	167	207	184	337
Ba	1041	663	842	1175	213	189	3	113	632	1317	224	612	85	54	144
Th	30	25	8.4	17	23	22	27	29	7.9	26	5.8	18	16	27	24
U	5.0	7.3	2.7	9.8	18	8.7	7.9	11	3.2	<1	6.1	1.6	4.5	12	14
Ta	1.4	0.8	0.9	1.3	2.7	2.5	1.4	3.6	1.0	1.1	0.6	1.2	1.4	1.5	3.8
Nb	41	29	11	17	24	26	16	19	10	11	10	6	18	16	17
Pb	24	15	26	19	23	23	31	35	14	22	18	23	20	38	22
Sr	314	562	326	411	58	48	5	27	196	647	94	327	22	13	39
Zr	155	61	178	223	76	70	98	74	135	190	70	93	154	133	106
Hf	4.1	2.2	4.9	5.5	3.2	3.1	3.7	3.7	3.6	7.4	2.6	2.3	5.8	5.5	4.7
Y	28	18	19	17	27	30	28	34	18	10	13	6.2	24	16	13
La	67	38	21	59	18	19	23	26	27	35	25	21	34	27	23
Ce	116	71	49	108	41	41	45	52	47	62	43	36	69	59	46
Pr	12	7.5	5.6	9.8	4.4	4.5	5.0	5.6	5.4	5.9	4.5	4.1	6.8	5.3	4.1
Nd	41	29	22	31	17	17	16	19	19	22	13	14	23	17	13
Sm	7.1	5.4	4.3	4.2	3.8	4.1	3.7	4.6	3.3	3.2	2.0	2.2	3.7	2.7	2.1
Eu	1.4	1.2	0.83	0.93	0.25	0.26	0.25	0.26	0.70	0.89	0.29	0.57	0.28	0.20	0.22
Gd	5.2	4.1	3.6	3.9	4.0	3.6	3.8	3.0	2.3	1.8	1.8	3.7	2.5	1.9	3.0
Tb	0.78	0.59	0.49	0.42	0.60	0.65	0.60	0.72	0.42	0.30	0.23	0.20	0.61	0.42	0.30
Dy	4.3	3.1	3.4	2.8	4.5	4.9	3.5	4.5	2.9	1.6	1.6	1.2	4.1	2.6	1.9
Ho	0.93	0.62	0.69	0.61	0.99	1.12	0.82	1.05	0.66	0.35	0.39	0.22	0.84	0.55	0.41
Er	2.4	1.5	2.1	1.9	3.1	3.5	2.3	2.7	2.0	0.95	1.3	0.59	2.6	1.7	1.5
Tm	0.39	0.22	0.30	0.30	0.46	0.55	0.36	0.46	0.30	0.15	0.24	0.09	0.46	0.30	0.25
Yb	2.5	1.4	2.0	2.0	3.1	3.5	2.4	2.9	2.0	0.93	1.6	0.52	3.0	1.9	1.8
Lu	0.40	0.21	0.32	0.33	0.49	0.61	0.35	0.44	0.34	0.15	0.30	0.09	0.47	0.32	0.27
Ga	16	19	19	20	15	15	17	16				16	14	11	15
10,000 × Ga/Al	2.13	2.29	2.40	2.40	2.04	2.04	2.04	1.64	1.95	1.92	1.92	2.41	2.41	2.49	2.84
ΣREE	261.64	163.32	225.09	101.10	105.13	107.07	124.61	114.08	136.63	95.41	82.28	151.42	121.87	96.33	93.52
(La/Yb)N	19.42	20.20	7.72	21.17	4.32	3.93	6.73	6.41	9.58	27.30	10.96	28.75	8.18	10.22	9.13
(La/Sm)N	6.17	4.60	3.22	9.09	3.10	3.05	3.92	3.72	5.35	7.12	8.05	6.06	5.84	6.64	7.02
(Gd/Yb)N	1.72	2.47	1.52	1.38	1.06	0.94	1.22	1.07	1.23	2.05	0.93	2.85	1.03	1.07	0.86
Eu/Eu [*]	0.68	0.72	0.63	0.74	0.20	0.19	0.21	0.19	0.67	0.95	0.45	0.85	0.23	0.33	0.17
Rb/Sr	0.57	0.28	0.36	0.31	3.44	4.37	53.60	9.85	0.53	0.10	1.82	0.29	7.57	12.32	5.26

Note. (La/Yb)N is chondrite-normalized La/Yb; (La/Sm)N is chondrite-normalized La/Sm; (Gd/Yb)N is chondrite-normalized Gd/Yb; Eu/Eu^{*} = Eu/N × 2/(SmN + GdN), where subscript N refers to chondrite-normalized value.

^aChen et al. (2013); b: Qiu et al. (2012); c: Li et al. (2012); d: Liu et al. (2012); e: Zhou and Yu (2001); f: Qiu et al. (2008).

TABLE A9 Whole rock Sr-Nd-Hf isotopic composition data from literature

Sample no.	Rb (ppm)	Sr		Sm (ppm)	Nd (ppm)	Lu		Hf (ppm)	Age (Ma)	Latitude
		87Sr/86Sr	Ratio			143Nd/144Nd _(i)	εNd _(t)			
Gunong	08JH332	0.708841	17	0.706600	0.512377	9	-3.90	0.30	4.14	0.282678
Changtai	08JH310	0.707155	15	0.706000	0.512408	11	-3.40	0.21	2.17	0.282697
Huxi	ZP-4			4.30	23.16	0.512405	9	-2.69		0.36
Huxi	ZP-5			4.22	32.27	0.512450	6	-3.24		96
Changqiao	ZP-6			17.02	17.02	0.512461	8	-2.43		24°08'
Xincun	08JH324					0.512352	11	-4.90	0.44	24°14'
Huacuo	Ta-2	220.80	33.92	0.739423	21	0.710228	0.512370	11	3.67	0.282642
Weitou	DS					0.512288	-4.10		9	24°37'
Quanzhou	Qf-1	61.13	242.10	0.707904	11	0.706785	0.512445	10	-2.50	111
Quanzhou	QZ-7									
Dacengshan	DCS-1			3.65	21.95	0.512308	9	-5.30		-2.35
Dacengshan	DCS-2			2.77	17.05	0.512301	11	-5.40		100
Nanzen	NZ-1			2.14	13.17	0.512295	10	-5.50		108
Nanzen	NZ-2			3.54	13.86	0.512325	9	-5.40		24°55'
Chengxi	ZP-8			11.53	11.53	0.512469	7	-2.68		-0.05
Sansha	SAN-1			2.95	15.45	0.512310	9	-5.40		96
Sansha	SAN-2			2.01	10.57	0.512320	6	-5.20		92

**FIGURE A1** Spider diagram of trace elements: (a) Group 1; (b) Group 2; and (c) Group 3 [Colour figure can be viewed at wileyonlinelibrary.com]